THERMODYNAMIC MODELING OF FLUIDS CONFINED IN POROUS MEDIA

A Thesis

by

NOURA ABDELKARIM ABDALLAH DAWASS

Submitted to the Office of Graduate and Professional Studies of
Texas A&M University
in partial fulfillment of the requirements for the degree of

MASTER OF SCIENCE

Chair of Committee,	Marcelo Castier
Co-Chairs of Committee,	Ioannis Economou
Committee Member,	Bing Guo
Head of Department,	M. Nazmul Karim

May 2016

Major Subject: Chemical Engineering

Copyright 2016 Noura Abdelkarim Abdallah Dawass

ABSTRACT

Fluids confined in porous media play a significant role in many engineering applications. Modeling fluids in oil reservoirs, adsorption based separations, and heterogeneous catalysis requires the accurate prediction of thermodynamic properties at a wide range of conditions. For confined fluids, this task involves accounting for the fluid-solid interactions induced by proximity to a solid wall. Most engineering models are only able to predict average properties of the system and fail to give information related to the heterogeneity of the confined fluid. Such information could be obtained through more rigorous but computationally expensive methods. In this work, an approach of intermediate complexity is developed to determine equilibrium properties of confined fluids, and to obtain local distribution of properties in the system. In this model, the variation of properties throughout the system takes place across regions that are defined depending on the effects present. Regions where confinement effects are important are further discretized into layers to capture local distribution within the confinement. For all elements, the volume is specified together with the temperature, and the total amount of each component. Thus, minimizing the Helmholtz energy determines the number of moles in each element; subsequently other properties are obtained. The Helmholtz energy accounts for internal interactions through an equation of state (EoS), in this work the Peng Robinson EoS is used. Additionally, the Helmholtz energy function includes an external contribution represented by an adsorption potential to account for fluid-solid interactions The Steele 10-4-3 potential was used for the confinement of light hydrocarbons in activated carbon. The prediction of local behavior was found to be comparable to the classical Density Functional Theory (DFT) calculations. Moreover, the Dubinin-Radushkevich-Astakhov

(DRA) potential was utilized to predict confinement of binary and ternary mixtures of methane, nitrogen, carbon dioxide on activated carbon, and the results were found to agree reasonably well with experimental data. Finally, the ability of the framework to model systems where confinement as well as other effects are present is demonstrated through predicting the molar distribution in a porous reservoir where gravitational effects are accounted for.

ACKNOWLEDGEMENTS

I would like to express my sincere gratitude to my advisors Professor Marcelo Castier and Professor Ioannis Economou. I am very fortunate to work and learn under the supervision of Professor Castier. His passion, curiosity and patience were essential for overcoming the difficulties faced during this research. I am also grateful for the guidance and support provided constantly by professor Economou. I am thankful for all the motivating words, kind advice and learning opportunities which contributed tremendously to my growth. My thanks extend to my committee member Dr. Bing Guo for his time and insightful comments which have improved this work. I would like to acknowledge the contributions made by Michelle D'Lima for this work. Throughout my research, her advice and support were very appreciated. Most importantly I am thankful for all the fun and amazing times I had working with her. Also, I would like to thank all the researchers, and students at TAMUQ for making my experience so memorable. Finally, I express my deepest gratitude to my family and friends. Thank you for the encouraging words, patience, and support.

This work was made possible by NPRP grant numbers $5-344-2-129$ and $6-1157-2-471$ from the Qatar National Research Fund (a member of the Qatar Foundation). The statements made herein are solely the responsibility of the authors.

NOMENCLATURE

Roman Letters

a – Molar Helmholtz energy $(T, V, \underline{x})$

A – Helmholtz energy (T, V, N)

A_{jm} – Helmholtz energy of a single grid

$A^{*,in}_{ijm}$ – Internal Helmholtz energy of component i in a grid

$A^{*,f}_{ijm}$ – External Helmholtz energy of component i in a grid

c – Volume translation parameter

$\hat{c}$ – Number of chemical components

$\Delta E^{j}_{F,i}$ – Summation of external field potentials of component i in layer j

f_{ℓ_m} – Number of external fields acting on layer j of each replica in region m

g – Molar Gibbs energy

$\hat{g}$ – Gravitational constant

h_{jm} – Depth of layer j in region m

H – Total pore width

H_{in} – Internal pore width (excluding the adsorbent radius, σ_s)

l_m – Number of layers in a given region

M_i – Molar mass of component i

N_{ads} – Absolute adsorbed amount

n^{*}_{ijm} – Number of moles of component i in all replicas of layer j in region m

n_i – Total number of moles of component i

$n_{f(l,m)}$ – Number of external fields acting on layer j in region m

P_0 – Reference pressure

P^{in} – Pressure calculated from a equation of state

$\hat{p}$ – Number of experimental data points

$\hat{r}$ – Number of regions

$\hat{r}_{conf}$ – Number of confined regions

r_m – Number of replicas in region m

R – Universal gas constant

T – System temperature

V_m – Total volume of region m

v_{jm} – Molar volume of layer j in region m

v_0 – Maximum porous volume

x_{ijm} – Mole fraction of the i^{th} component layer j in region m

z_{jm} – Distance from the center of the pore to the confining wall

Greek Letters

β – Solid heterogeneity parameter

Γ – Surface excess

δ – Kronecker delta function

Δ – Interlayer spacing of the adsorbent

$\varepsilon_{s,i}$ – Solid-fluid energy interaction parameter

ε_0 – Characteristic energy

θ^*_{ijm} – Distribution factor

μ_i – Chemical potential of component i

ρ_s – Density of the solid (adsorbent)

$\sigma_{s,i}$ – Solid-fluid diameter

Subscripts

i – Component

j – Layer

k – Component (Gradient)

l – Component (Hessian)

m – Region

MAX – Dependent variable

Superscripts

$*$ – Total amounts of all replicas

f – External field contribution

in – Internal field contribution

TABLE OF CONTENTS

LIST OF FIGURES

LIST OF TABLES

TABLE Page

1. INTRODUCTION

The study of fluids confined in small pores is significant for many scientific and industrial applications, including various sectors of the oil and gas industry. Upstream operations such as well characterization, well testing, and production require modeling of oil and gas in porous reservoirs. Currently, recovering natural gas from unconventional reservoirs, such as coalbed and shale reservoirs, requires information on the adsorption behavior of the confined gas [1]. Similarly, downstream treatment of oil and gas to obtain petroleum products is achieved through the use of porous materials for separation, purification, and catalysis. Examples of generic commercial adsorbents include activated carbon, activated alumina, zeolites, and silica gel [2]. These materials are comprised of pores with sizes in the range of nanometers. As a result it is crucial to account for the confinement effect when studying fluids in these systems. Furthermore, the need for more environment friendly technologies has motivated the development of new and more advanced materials. One class of porous materials that has high selectivity is molecular organic frameworks (MOFs). Currently, different types of MOFs are designed and investigated for many applications, including replacing energy intensive technologies for challenging separations [3].

In order to successfully design, operate, and improve any process, the accurate prediction of thermodynamic properties is required. For applications with confined fluids, knowledge of the adsorptive capacity of microporous materials is needed. In particular, adsorption isotherms, which provide the equilibrium amount of a particular component or mixture adsorbed at a specific temperature and pressure range, is of extreme importance [4–6]. In these applications, fluids are trapped in materials with meso-pores (2-50 nm) and micro-pores (less than 2 nm), where the proximity to the solid wall must be accounted for. Specifically, theoretical studies of such systems have to consider the solid-fluid interactions, and the size of the pores [7, 8]. Moreover, the confined fluids models should be able to account for the non-ideality of the fluid, and eventually predict multicomponent adsorption at a wide range of temperatures and pressures. Nonetheless, even if these interactions are accounted for, most available models compute the average or global properties of the confined systems.

Assuming uniform behavior in the porous space ignores the heterogeneity of the fluid, or the local distribution of the fluids properties. For confined fluids, non-uniform behavior exists due to many effects, including the variation of the fluid properties with distance from the wall, and the presence of different sizes or geometries within the same porous space. Accounting for multiple effects is particularly useful for separating the geometry effects in solids composed of spherical cavities connected by cylindrical channels, as in the case of MOFs. Other than these microscopic effects, confined fluids could be subject to effects at a larger scale. For instance, gravity creates a molar distribution of the components in deep oil reservoirs along the depth of the formation. As a result, including the gravitational and confinement effects simultaneously will give a better representation of the properties of the components in these systems.

The objective of this work is to establish a general framework for determining equilibrium properties of fluids in confined media. The thermodynamic model utilizes an EoS to describe both the bulk and confined phases. On the other hand, the confinement effect could be represented for any solid, regardless of its shape or size, provided that an appropriate model to describe the solid-fluid interactions is available. Another goal is to find equilibrium conditions when several effects are acting on the system, whether they arise from the nature of the confined media or from other sources.

Based on these objectives, the thesis outline is as follows: in section 2, a literature review of the various theoretical approaches of studying confined fluids is presented. By comparing this work to the currently available methods, the review highlights the advantages and limitations of the proposed method. Sections 3 and 4 describe the methodology followed in this work. In section 3, the formulation of the model is provided, including details related to the EoS and potentials selected to represent the systems considered in this work. Then, using the required model functions and equations, a solution can be obtained. The solution method and tools employed in this work is described in section 4, along with a discussion of the main difficulties faced when solving the model. The results of implementing the solution and testing the established framework are presented in section 5. This involves comparisons with experimental data, and similar works. Finally, the main findings are examined in the conclusions section, followed by section 7 that explores future possibilities associated with the model established here.

2. LITERATURE REVIEW OF CONFINED FLUIDS MODELS

2.1 Empirical and Ideal Models

Over the years, many adsorption models have been developed with different capabilities, assumptions, and levels of complexity. Initially, equilibrium isotherms for pure components were obtained through ideal models that are largely applied due to their simplicity. Ideal models could assume an ideal solid phase, or a homogeneous solid. In literature, homogeneous solids refer to the assumption that the energy of adsorption sites is the same everywhere. On the other hand, in heterogeneous or real solids, adsorption sites have an energy distribution among them. Another assumption that is utilized by most ideal models is the assumption of ideal adsorbed phase. In other words, the molecule-molecule interactions of the confined fluid are not accounted for [4]. One of the earliest empirical equations is the Langmuir isotherm model, which was developed in the early twentieth century. This famous model considers the localized adsorption of molecules at certain sites on the solid surface [9].

Following Langmuir's approach, other localized isotherms were later developed including Toth equation, Sips equation, Jovanovich equation and many other models [10–12]. While they account for the solid heterogeneity through constants correlated to experimental data, still they share many deficiencies with Langmuir's isotherm. Mainly, they all assume an ideal adsorbed phase, and that the adsorbed amount on the surface of a single component is not affected by the presence of other components. As a result, these models are not suitable for describing mixtures. Later on, fluid adsorption on solid surfaces was visualized through more advanced mechanisms, as in the case of multilayer adsorption models. The most common multilayer equation is the Brunauer-Emmett-Teller (BET) isotherm which is widely used for surface area determination [13]. Even more sophisticated is the description of adsorption through a pore filling mechanism that formed the basis for correlations like the Kelvin equation and Dubinin equations, including the DRA equation [14–16].

2.2 Adsorbed Solution Theory Models

In general, localized isotherms and the equations formulated by Dubinin were used to obtain pure component isotherms by assuming an ideal fluid. Some of these equations were extended to describe confined fluid mixtures since most engineering applications involve mixtures. However, these models showed serious deficiencies when applied to mixtures [2,4,5]. In 1965, Myers and Prausnitz published the Ideal Adsorption Solution Theory (IAST) [17] following a thermodynamic approach to the adsorption problem. IAST represents a milestone in the development of adsorption models, due to its sound theoretical basis and its ability to predict multicomponent adsorption equilibria based on experimental data of pure components. Additionally, the theory presented a simple framework that allows the incorporation of other adsorption models to account for the heterogeneity, or non-ideality, of the solid phase [18–21]. Subsequently, during the 1980s, many attempts to enhance IAST prediction by accounting for fluid molecular interactions emerged, such as the works of Myers [22], Costa et al. [23], and Sochard et al. [24] These models are referred to as Real Adsorbed Solution Theory (RAST), where the activity coefficients are correlated using multicomponent experimental data, which results in the loss of the predictive feature of the adsorbed solution theory [25].

2.3 Molecular Approaches

The same decade witnessed the emergence of another class of models for confined fluids, namely models based on the classical DFT [26–29]. Rooted in statistical mechanics, DFT models are constructed by expressing the free energy of an inhomogeneous fluid as a functional of the density. Then, the density profile, and subsequently any other thermodynamic property, is obtained by minimizing the free energy functional. Hence, the theory provides a rigorous framework to modeling fluids in the bulk and confined phases and predicting phase related phenomena, such as capillary condensation [30]. In addition to DFT, many statistical based methods have the ability to describe local density distribution and phase transitions, including grand canonical Monte Carlo simulation (GCMC) [31–35]. The use of such methods is still hindered by their high computational cost, which makes them unfeasible for conventional engineering calculations. Nonetheless, understanding confined fluids through molecular approaches could be utilized by more practical models. As an example, DFT models and simulation works utilize intermolecular potential functions to describe fluid-solid interactions and some of these functions are adopted by some engineering models [36].

2.4 Engineering Models

By the end of the twentieth century, less computationally demanding methods were developed to study fluids in porous media. In 1998, Shapiro and Stenby [37] adopted the Potential theory [38] for multicomponent adsorption, which assumes that the adsorbed fluid is experiencing a potential field emitted by the solid surface. The variation of the adsorption potential in the porous space results in a density distribution. In the multicomponent potential theory of adsorption (MPTA), the chemical potential is modified to include an adsorption potential with an EoS used to model components in the adsorbed and bulk phase.

The adsorption potential used depends on the solid type and geometry. Shapiro and Stenby [37] extended the DRA equation to multicomponent systems. The DRA equation can be used for any geometry or solid, given that pure component experimental data are available. The MPTA-DRA model was used to model the adsorption of pure components and mixtures on activated carbon [39–41], molecular sieves [40], and MOFs [42]. Additionally, other than adsorption correlations, intermolecular potentials could be utilized as in the case of the Steele potential which was used to model fluids adsorbed in slit shaped activated carbon pores [39, 41]. Regardless of the potential applied, MPTA is considered a predictive model, in the sense that only pure component data are fitted and are then used to describe mixtures [25, 39].

Another practical approach to adsorption calculations involves the extension of an EoS. This approach was developed by Travalloni et al. [7, 43, 44], Islam et al. [45], and Piri [46] These various publications show the ability of modified EoS to predict the thermodynamic properties of confined fluids, including pore condensation and critical point shift. However, such equations often follow a mean field approach to describe fluids, and thus are not suitable for studying local behavior.

3. MODEL FORMULATION

In order to model fluids in confined media, the fluid is considered to experience a field emitted by the solid wall as postulated by the potential theory put forward by Polanyi [38]. The intensity of this potential changes with distance, thus creating a heterogeneous or non-uniform distribution of the properties of the adsorbed fluids. For instance, the density of the confined fluid changes as a function of distance, as illustrated in Figure 3.1. To account for the various effects or fields imposed, and capture the heterogeneous behavior the system studied is discretized.

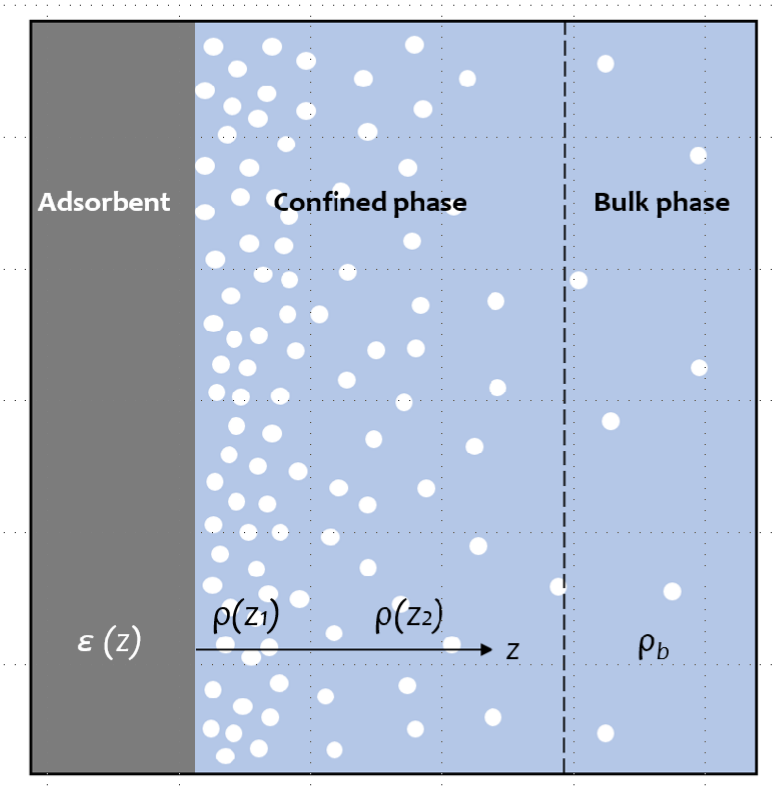

Figure 3.1: Example of an inhomogeneous fluid resulting from an adsorption potential.

3.1 System Discretization

In the case of adsorption, the confined fluid coexists with a bulk phase where no external effects are present. As a result, in this model the system is divided into regions depending on the external effects present. For example, in adsorption problems, the bulk region does not experience any effects so it is separated from the confined region. Furthermore, when a field is present, the region is divided into layers in the direction perpendicular to the field to be able to obtain the distribution of properties in that direction as in Figure 3.2. For some problems, fields acting with different directions might act on a region, thus requiring the region to be divided into grids.

In this work, fields with different directions could be considered. Other than the directions considered, the shape and volume of layers or grids also depend on the geometry of the region. As a result, when a field is acting on a region, the geometry should be specified as slit, cylindrical, or spherical. Then, the region is further discretized to layers corresponding to the geometry specified. Several possibilities exist for discretization but, in this work the layers have equal volume. Moreover, for systems with multiple identical pores, replicas of a single confined region (single pore) are created. The number of replicas is determined from the total porous volume. In this model, the volume of each region and volumes of the layers are specified and fixed. Other specifications include the temperature and the total amounts, or number of moles of each component in the system.

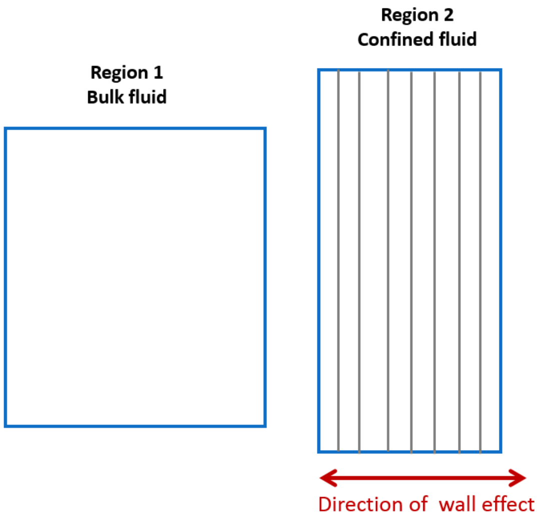

Figure 3.2: Example of discretization for a system under the effect of one field.

3.2 Helmholtz Energy

Selecting the independent variables to be the temperature (T), volume (V), and total amounts (N) for a closed system dictates that the minimum Helmholtz energy of the system corresponds to the equilibrium state of the system, as a result of the second law of thermodynamics [47]. Finding the Helmholtz energy at equilibrium will determine how each component is distributed within layers and regions of the system, consequently yielding the density distribution. Also, determining the Helmholtz energy allows the computation of other thermodynamic properties, using fundamental thermodynamic relations.

The total Helmholtz energy of the system, A, is found by summing the Helmholtz energy of each layer in each region, as in the following equation,

$$A = \sum_{m=1}^{\hat{r}} \sum_{j=1}^{\ell_m} r_m A_{jm} \tag{3.1}$$

where $\hat{r}$ is the number of regions, r_m is the number of replicas of region m, ℓ_m is the number of layers in each replica of region m, and A_{jm} is the Helmholtz energy of layer j in each replica in region m. Defining A^*_{jm} as the joint contribution of all replicas of layer j in region m, i.e.:

$$A^*_{jm} = r_m A_{jm} \tag{3.2}$$

equation 3.1 then takes the form:

$$A = \sum_{m=1}^{\hat{r}} \sum_{j=1}^{\ell_m} A^*_{jm} \tag{3.3}$$

The Helmholtz energy can be split in an internal contribution, associated with the equation of state, and a contribution due to the effect of external fields, i.e.:

$$A^*_{jm} = A^{*,in}_{jm} + A^{*,f}_{jm} \tag{3.4}$$

where the superscripts *in* and f denote the internal and field contributions, respectively. The total field contribution may result from the simultaneous effect of multiple individual fields, which give rise to layers in different directions within a given region. Thus, equation 3.4 can be rewritten as:

$$A = \sum_{m=1}^{\hat{r}} \sum_{j=1}^{\ell_m} \left(A^{*,in}_{jm} + \sum_{f=1}^{f_{\ell_m}} A^{*,f}_{fjm} \right) \tag{3.5}$$

where f_{ℓ_m} represents the number of external fields acting on layer j of each replica in region m.

As discussed later on, the procedure for minimization of the Helmholtz energy requires first and second derivatives A^*_{jm} with respect to mole numbers. The first derivative is given by:

$$\mu^*_{ijm} = \left(\frac{\partial A^*_{jm}}{\partial n^*_{ijm}}\right)_{T,V^*_{jm},n^*_{\neq i,jm}} = \left(\frac{\partial A_{jm}}{\partial n_{ijm}}\right)_{T,V_{jm},n_{\neq i,jm}} = \mu_{ijm} \tag{3.6}$$

where μ^*_{ijm} is the chemical potential of component i, in grid j of region m, and n^*_{ijm} is the number of moles in that grid, considering all replicas and the effect of all fields. The notation $\neq i$ indicates components other than i. To derive the two rightmost terms of Eq. 3.6, we note that the relationship between n^*_{ijm} and n_{ijm}, which is the corresponding amount in a single replica, follows:

$$n^*_{ijm} = r_m n_{ijm} \tag{3.7}$$

Using equation 3.7, the second derivative of A^*_{jm} with respect to mole numbers is given by:

$$\left(\frac{\partial}{\partial n^*_{kjm}}\left(\frac{\partial A^*_{jm}}{\partial n^*_{ijm}}\right)_{T,V^*_{jm},n^*_{\neq i,jm}}\right)_{T,V^*_{jm},n^*_{\neq k,jm}} = \left(\frac{\partial \mu^*_{ijm}}{\partial n^*_{kjm}}\right)_{T,V^*_{jm},n^*_{\neq k,jm}} = \frac{1}{r_m}\left(\frac{\partial \mu_{ijm}}{\partial n_{kjm}}\right)_{T,V_{jm},n_{\neq k,jm}} \tag{3.8}$$

Finally, the first and second derivatives of A^*_{jm} are the result of adding the derivatives of the internal and external contributions in that element. The following subsections discuss the evaluation of the internal and external field contributions.

3.2.1 Internal Contribution to the Helmholtz Energy

For this model, the internal contribution to the Helmholtz energy accounts for fluid-fluid interactions. This work considers two possibilities when deriving the internal contribution depending on the EoS expression used. The first possibility is to use the expression of the molar residual Helmholtz energy. The molar residual Helmholtz energy is defined here as the difference between the molar Helmholtz energies of the fluid and of the ideal gas at the same temperature, molar volume, and component mole fractions, i.e.:

$$a^{res}\left(T, v, \underline{x}\right) = a\left(T, v, \underline{x}\right) - a^{ig}\left(T, v, \underline{x}\right) \tag{3.9}$$

For EoS models where the explicit expression for $a^{res}\left(T, v, \underline{x}\right)$ is known, the internal contribution to the Helmholtz energy is derived following the four-state path in Figure 3.3.

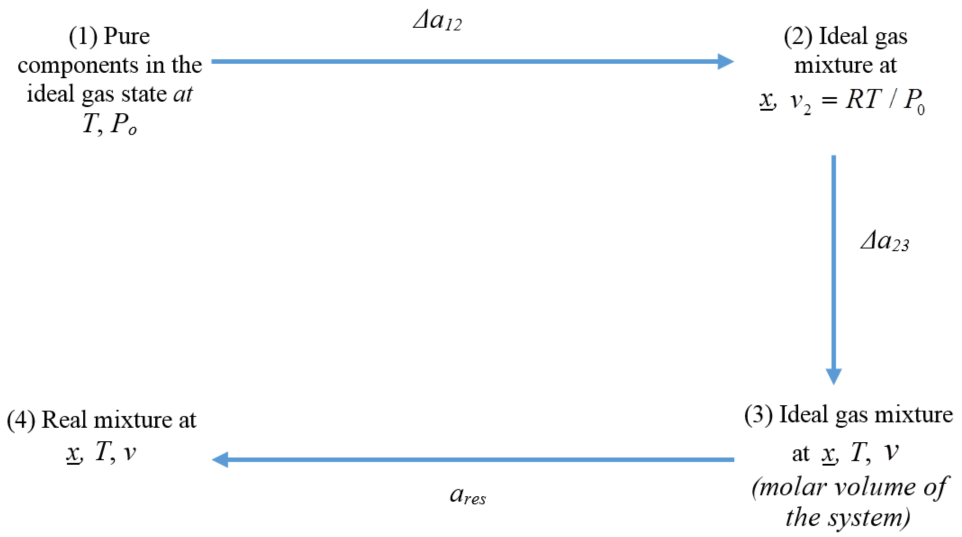

Figure 3.3: Schematic representation of the thermodynamic path describing the change in Helmholtz energy when using the molar residual Helmholtz energy.

The effect on the molar Helmholtz energy of forming an ideal gas mixture isothermally (State 2) from the pure components (State 1) can be computed as follows:

$$\Delta a_{12} = \Delta g_{12}^{ig} - \Delta\left(Pv^{ig}\right)_{12} = RT\sum_{i=1}^{\hat{c}} x_i \ln x_i - R\Delta T = RT\sum_{i=1}^{\hat{c}} x_i \ln x_i \tag{3.10}$$

where $\hat{c}$ denotes the number of components and g is the molar Gibbs energy. The change between states 2 and 3 is given by:

$$\Delta a_{23} = \int_{v_2}^{v} \left(\frac{\partial a}{\partial v}\right)_{T,}^{ig} dv = -RT\int_{v_2}^{v} \frac{1}{v} dv = -RT \ln \frac{P_0 v}{RT} \tag{3.11}$$

The molar Helmholtz energy change between states 3 and 4 is the residual molar Helmholtz energy, $a^{res}\left(T, v, \underline{x}\right)$, whose expression depends on the model adopted for a given calculation. Reintroducing the indexes for region and layer, the expression for the Helmholtz energy is:

$$A_{jm}^{*,in} = RT\left[\sum_{i=1}^{\hat{c}} n_{ijm}^{*} \ln x_{ijm} - \left(\sum_{i=1}^{\hat{c}} n_{ijm}^{*}\right)\left(\ln \frac{P_0 v_{jm}}{RT} - \frac{a^{res}\left(T, v_{jm}, \underline{x}_{jm}\right)}{RT}\right)\right] \tag{3.12}$$

where $\underline{x}_{jm}$ denotes the vector of mole fractions of all components in layer j of region m.

The relationship between n_{ijm}^{*} and n_{ijm}, which is the corresponding amount in a single replica, is given in equation 3.7. For the mole fractions and molar volumes, it holds that:

$$x_{ijm}^{*} = x_{ijm} \tag{3.13}$$

$$v_{jm}^{*} = v_{jm} \tag{3.14}$$

For this reason, the superscript $*$ does not appear in these variables in equation 3.12.

When an expression for P^{in} from an EoS is used, the internal contribution to the Helmholtz energy is also obtained following the four-state path depicted in Figure 3.4. The molar Helmholtz energy change between states 1 and 2 is given by Eq. 3.10. To compute the effect of expanding the ideal gas to infinite volume, one can use:

$$\begin{gathered}\Delta a_{23} = \int\limits_{v_2}^{\infty} \left(\frac{\partial a}{\partial v}\right)_{T,\underline{x}}^{ig} dv = -RT\left[\int\limits_{v_2}^{v} \frac{1}{v}dv + \int\limits_{v}^{\infty} \frac{1}{v}dv\right] = \\ -RT\ln\frac{v}{v_2} - RT\int\limits_{v}^{\infty}\frac{1}{v}dv = -RT\ln\frac{P_0 v}{RT} - RT\int\limits_{v}^{\infty}\frac{1}{v}dv\end{gathered} \tag{3.15}$$

In the final step, the fluid is taken from infinite molar volume to its molar volume, i.e.:

$$\Delta a_{34} = \int\limits_{\infty}^{v}\left(\frac{\partial a}{\partial v}\right)_{T,\underline{x}} dv = -\int\limits_{\infty}^{v} P^{in} dv \tag{3.16}$$

where P^{in} represents the pressure as computed by the underlying EoS used to model the internal contribution to the bulk fluid behavior.

Adding these various terms and reintroducing the indexes that denote the region and layer, the expression for the Helmholtz energy is:

$$A_{jm}^{*,in} = RT\left[\sum_{i=1}^{\hat{c}} n_{ijm}^{*}\ln x_{ijm} - \left(\sum_{i=1}^{\hat{c}} n_{ijm}^{*}\right)\left(1 + \ln\frac{P_0 v_{jm}}{RT} + \int\limits_{\infty}^{v_{jm}}\left(\frac{P_{jm}^{in}}{RT} - \frac{1}{v_{jm}}\right)dv_{jm}\right)\right] \tag{3.17}$$

where n_{ijm}^{*} represents the total amount of component i in all replicas of layer j in region m.

The final expression for $A_{jm}^{*,in}$ is dependent on the chosen EoS. In this work, the Peng-Robinson EoS with volume translation is used. Also, the first and second derivatives of the internal Helmholtz energy are required and obtained through,

$$\mu^*_{ijm} = RT\left[\ln x_{ijm} - \ln\frac{P_0 v_{jm}}{RT} - \frac{\partial}{\partial n^*_{ijm}}\left[\left(\sum_{p=1}^{\hat{c}} n^*_{pjm}\right)\int_{\infty}^{v}\left(\frac{P^{in}_{jm}}{RT} - \frac{1}{v_{jm}}\right)\partial v_{jm}\right]\right] \tag{3.18}$$

$$\frac{\partial \mu^*_{ijm}}{\partial n^*_{kjm}} = RT\left[\frac{1}{\left(\sum\limits_{p=1}^{\hat{c}} n^*_{pjm}\right)}\frac{\delta_{ik}}{x_{ijm}} - \frac{\partial^2}{\partial n^*_{ijm}\partial n^*_{kjm}}\left[\left(\sum_{p=1}^{\hat{c}} n^*_{pjm}\right)\int\limits_{\infty}^{v}\left(\frac{P^{in}_{jm}}{RT} - \frac{1}{v_{jm}}\right)\partial v_{jm}\right]\right] \tag{3.19}$$

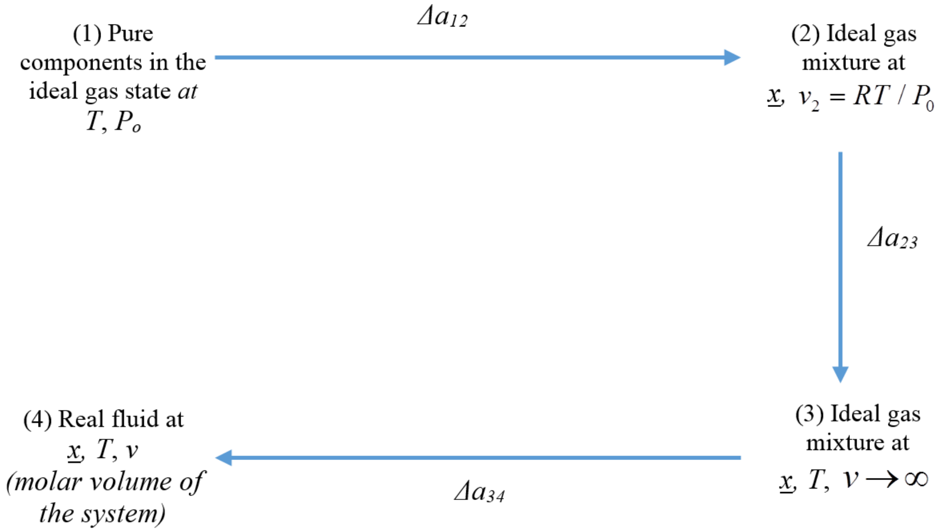

Figure 3.4: Schematic representation of the thermodynamic path describing the change in Helmholtz energy when using an EoS.

3.2.1.1 Peng-Robinson EoS

Volume translated Peng-Robinson EOS [48, 49] is used in this work. Volume translation [50] is used to improve density predictions of the EOS, which has the following expression,

$$P = \frac{RT}{v + c_m - b_m} - \frac{a_m}{(v + c_m)(v + c_m + b_m) + b_m (v + c_m - b_m)} \tag{3.20}$$

Parameters a_m, b_m and c_m are determined using:

$$a_m = \sum_{i=1}^{\hat{c}} \sum_{j=1}^{\hat{c}} x_i x_i a_{ij} \tag{3.21}$$

$$a_{ij} = \sqrt{a_i a_j}\,(1 - k_{ij}) \tag{3.22}$$

$$b_m = \sum_{i=1}^{\hat{c}} x_i b_i \tag{3.23}$$

$$c_m = \sum_{i=1}^{\hat{c}} x_i c_i \tag{3.24}$$

where k_{ij} is a binary interaction parameter. The expressions for a_i, b_i and c_i are:

$$a_i = 0.45724 \frac{\alpha_i R^2 T_{ci}}{{P_{ci}}^2} \tag{3.25}$$

$$\alpha_i(T) = [1 + (1 - T_{ri}^{0.5})(0.37464 + 1.5422\omega_i - 0.26992\omega_i^2)]^2 \tag{3.26}$$

$$b_i = 0.07780 \frac{RT_{ci}}{P_{ci}} \tag{3.27}$$

where T_{ci}, P_{ci}, and ω_i are the critical temperature, critical pressure, and acentric factor of component i. The symbol T_{ri} stands for the reduced temperature of component i, which is equal to:

$$T_{ri} = \frac{T}{T_{ci}} \tag{3.28}$$

Finally, c_i, which is related to volume translation is found using,

$$c_i = s_i b_i \tag{3.29}$$

where the shift parameter s_i is determined using liquid densities experimental data and its value is generally negative.

3.2.2 External Contribution to the Helmholtz Energy

The external contribution to the Helmholtz energy accounts for the fluid-solid interactions, or the effect of the solid adsorbent on the fluid. This effect changes with distance, and is described through an adsorption potential.

3.2.2.1 The Steele Potential

In this work, the Steele 10-4-3 potential [51] is applied to model fluids in activated carbon with microscopic, slit-like pores. Figure 3.5 shows the energy function that describes the interactions between the solid wall and adsorbed molecules. In slit pores, two solid walls contribute to the potential. Consequently, at each layer in a region subjected to a confining wall, the field contribution of the Helmholtz energy is computed by,

$$A^f_{jm} = A^f_{jm}(z) + A^f_{jm}(H - z) \tag{3.30}$$

where, H is the wall to wall distance. For each wall, the Steele contribution at distance z is,

$$A^{f,*}_{jm}(z) = 2\pi\rho_s\Delta\sum_{i=1}^{\hat{c}} n^*_{ijm}\left[\varepsilon_{s,i}\sigma^2_{s,i}\left[\frac{2}{5}\left(\frac{\sigma_{s,i}}{z_{jm}}\right)^{10} - \left(\frac{\sigma_{s,i}}{z_{jm}}\right)^4 - \frac{\sigma^4_{s,i}}{3\Delta(0.61\Delta + z_{jm})^3}\right]\right] \tag{3.31}$$

where ρ_s and Δ are the solid density and solid interlayer spacing respectively. The combined size of the solid and fluid molecules, $\sigma_{s,i}$, and the combined energy, $\varepsilon_{s,i}$, are calculated using the Lorentz-Berthelot combining rules,

$$\sigma_{sf,i} = \frac{\sigma_s + \sigma_{f,i}}{2} \tag{3.32}$$

$$\varepsilon_{sf,i} = (\varepsilon_s\varepsilon_{f,i})^{1/2} \tag{3.33}$$

while the fluid molecular diameter, $\sigma_{f,i}$, is found from the b parameter of the EoS [52],

$$\sigma_f = \left(\frac{3b}{2\pi N_A}\right)^{1/3} \tag{3.34}$$

and the energy parameter $\varepsilon_{sf,i}$ is used to characterize adsorption of the i^{th} component in a given solid and is found by fitting experimental data of that system.

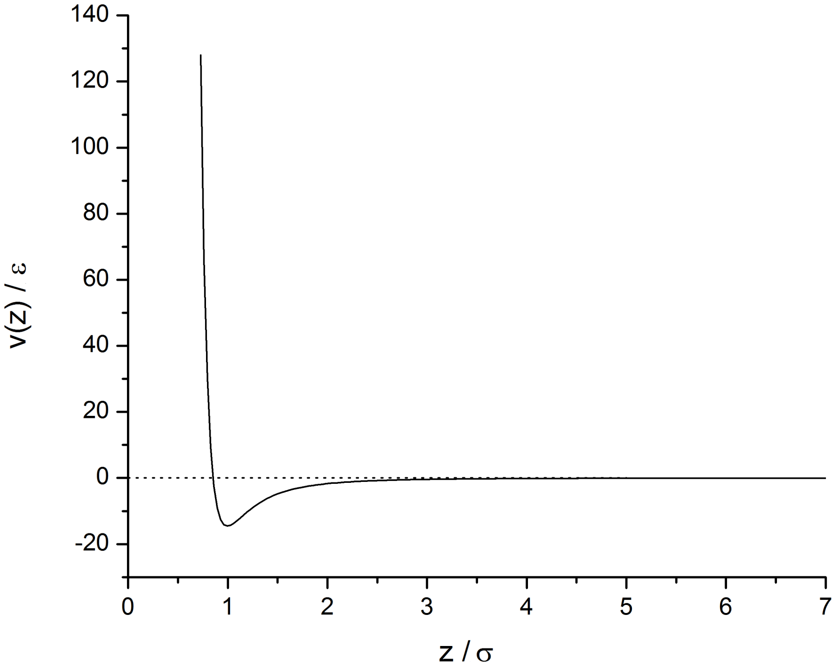

Figure 3.5: Solid-fluid interaction potential vs. dimensionless distance.

3.2.2.2 The Dubinin-Radushkevich-Astakhov Potential

Another potential used to describe the effect of a confining wall is the Dubinin-Radushkevich-Astakhov (DRA) potential [15,16]. The potential was originally used to correlate the adsorbed volume of pure vapor, v, and the adsorption energy, ε,

$$v = v_o \exp\left[\left(\frac{\varepsilon}{\varepsilon_o}\right)^{\beta}\right] \tag{3.35}$$

where, v_o is the maximum porous volume and ε_o is the characteristic energy of adsorption. The parameter β is related to the solid heterogeneity, and for activated carbon, β takes on the value of 2. Equation 3.35 was proposed by Dubinin without taking into account the change of properties with distance in the porous space.

Shapiro and Stenby [37] implemented a modification to account for the heterogeneity of the adsorbed component. The DRA equation is also extended for multicomponent adsorption. The potential experienced by each component, ε_i, is given by,

$$\varepsilon_i = \left[-\varepsilon_{oi} \left(\ln \left[\frac{v_o}{v} \right] \right)^{1/\beta} \right] \tag{3.36}$$

where the calculations are performed over the porous volume from $v = 0$ to $v = v_o$. In general, the DRA potential does not require the geometry of the pore to be specified, unlike the Steele potential. However, the methodology of this work requires the shape of the confined region to be explicitly specified as input. Therefore, for slit pores a pore width, H, is defined and v_o is used to define the volume of the region. Additionally, the calculations assume the adsorption due to a single wall and are performed from $z = 0$ to $z = H$, as in Figure 3.6. According to the potential, when z approaches H, the adsorption energy approaches zero or in other words, the fluid approaches bulk fluid behavior. As a result of the assumptions followed in this framework, the adsorption contribution to the Helmholtz energy in each layer is calculated at each distance,z_{jm}, as,

$$A^{*,f}_{jm} = -\sum_{i=1}^{\hat{c}} n^*_{ijm} \left[\varepsilon_{0i} \left(\ln \left[\frac{H}{z_{jm}} \right] \right)^{1/\beta} \right] \tag{3.37}$$

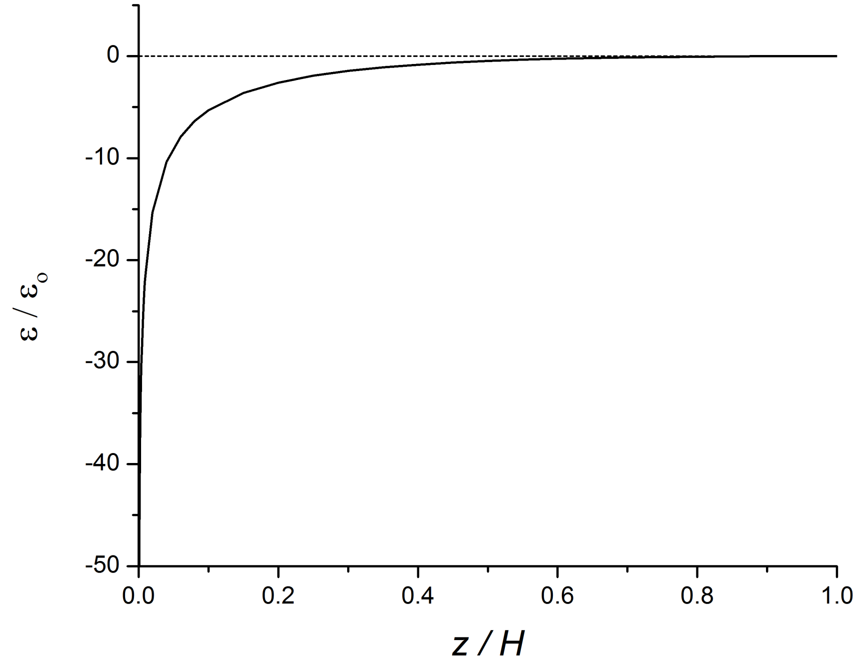

Figure 3.6: Energy vs. distance of the DRA potential.

3.2.2.3 Gravitational Field

The effect of the gravitational field is relevant to compositional grading, in which the pressure and composition of a mixture change with the vertical position coordinate, like depth in an oil reservoir. In calculations where it is desired to model confined fluids while accounting for the effect of gravity the potential contribution is added to the Helmholtz energy,

$$A^{*,f}_{jm} = \hat{g} h_{jm} \sum_{i=1}^{\hat{c}} n^{*}_{ijm} M_i \tag{3.38}$$

where M_i is the molar mass of component i and h_{jm} is the height of layer j in region m.

4. MODEL SOLUTION

4.1 Numerical Methods

The objective of the model derived in the previous section is to find the distribution of the amount of each component by minimizing the Helmholtz energy of the considered system. The solution is obtained numerically, given that the functional form of the objective function, A/RT, is complicated and that the optimization is performed with respect to a large number of variables. The numerical optimization method used in this work is a second order Newtons method, modified based on Cholesky factorization. The full algorithm of this method is found in Murray [53].

For this problem, the variables to be optimized should be the number of moles in each element. However, instead of changing the number of moles with every iteration, it is convenient to vary dimensionless and normalized quantities. Consequently, the distribution factor, θ_{ijm}, is introduced to the equilibrium problem and is defined as,

$$\theta^*_{ijm} = \frac{n^*_{ijm}}{n_i} \tag{4.1}$$

In equation 4.1, n_{ijm} is the number of moles of the i^{th} component in layer j of region m, and n_i is the total number of moles of the i^{th} component in the system.
Due to conservation of mass, note that for each component i:

$$\sum_{m=1}^{\hat{r}} \sum_{j=1}^{\ell_m} \theta^*_{ijm} = 1 \tag{4.2}$$

Thus, it is possible to adopt one of the θ values of component i as a dependent variable. In this work, the largest θ value is considered to be dependent, denoted by $\theta^*_{i,MAX}$ and computed as,

$$\theta^*_{i,MAX} = 1 - \left(\sum_{m=1}^{\hat{r}} \sum_{j=1}^{\ell_m} \theta^*_{ijm} \right)_{\neq MAX} \tag{4.3}$$

The subscript $\neq MAX$ on the right hand side of Eq. 4.3 indicates that all θ values of component i are added, except the dependent or the largest one. In practice, at the beginning of each iteration, the largest θ value of each component i is flagged as a dependent variable and the numerical procedure generates new values for all the independent θ values. Then, the dependent, or largest, value is computed again using Eq. 4.3, allowing the evaluation of the objective function and its derivatives during the subsequent iteration. Ultimately, assigning a dependent variable for each component will result in the number of variables to be computed as,

$$n_{\text{var}} = \hat{c} \left(\left(\sum_{m=1}^{\hat{r}} m l_m \right) - 1 \right) \tag{4.4}$$

The optimization requires the computation of the gradient vector and the Hessian matrix, which are found by computing the first and second derivatives of the Helmholtz function with respect to the distribution factors, respectively. Expressions for derivatives of A/RT with respect to the number of moles were presented in section 3. In the following equations, the g vector and H matrix elements are expressed in terms of number of moles derivatives,

$$\frac{\partial A}{\partial \theta^*_{ijm}} = n_i \left(\mu^*_{ijm} - \mu^*_{iJM} \right) \tag{4.5}$$

where the lowercase subscripts refer to the the independent layers of component i, while the capital subscripts represent the dependent layers of component i.

$$\begin{aligned}\frac{\partial^2 A}{\partial \theta^*_{i,ji,mi} \partial \theta^*_{l,jl,ml}} &= n_i n_l \left[(\delta_{mi,ml}\delta_{ji,jl} - \delta_{mi,ML}\delta_{ji,JL}) \left(\frac{\partial \mu^*_{i,ji,mi}}{\partial n^*_{l,ji,mi}} \right) \right] \\ -n_i n_l & \left[(\delta_{MI,ml}\delta_{JI,jl} - \delta_{MI,ML}\delta_{JI,JL}) \left(\frac{\partial \mu^*_{i,JI,MI}}{\partial n^*_{l,JI,MI}} \right) \right]\end{aligned} \tag{4.6}$$

where δ represents the Kronecker delta.

For each iteration, the gradient and the Hessian are used to calculate a new solution vector. This iterative procedure is stopped when the elements of the gradient reach close to zero, within a specified tolerance, corresponding to the minimum of the Helmholtz energy. Specifically, in order to stop the energy minimization, the difference between the maximum absolute value in the gradient and zero should be less than $1\text{x}10^{-12}$.

4.2 Initial Estimates

Like many numerical solutions, the optimization procedure described above requires a good initial estimate to start the calculations. Assuming ideal gas behavior will simplify the problem, and allow for the number of moles in each layer of the system to be found analytically. Here, the derivation of the ideal gas solution is illustrated through a simple system that is composed of one region (hence, the region subscript was dropped for this example) and two layers, denoted by subscripts A and B. Also, it is assumed that the system contains two components, denoted by subscripts 1 and 2. For each component, the modified chemical potential (which includes the external potentials) of all the layers in the system should be the same, at equilibrium. For component 1,

$$\frac{\mu_{1A}}{RT} = \frac{\mu_{1B}}{RT} \tag{4.7}$$

For ideal gas, the modified chemical potential is expressed as,

$$\ln x_{1A} + \ln P_A + \frac{1}{RT}\frac{\partial A_{1A}^{*,f}}{\partial n_{1A}^*} = \ln x_{1B} + \ln P_B + \frac{1}{RT}\frac{\partial A_{1B}^{*,f}}{\partial n_{1B}^*} \tag{4.8}$$

where $\frac{\partial A_{1A}^{*,f}}{\partial n_{1A}^*}$ is the sum of external field potentials applied in layer A, for component 1. Then, taking the natural logarithm and rearranging equation 4.8 yields,

$$\frac{x_{1A}P_A}{x_{1B}P_B} = \exp\left(\frac{1}{RT}\left(\frac{\partial A_{1B}^{*,f}}{\partial n_{1B}^*} - \frac{\partial A_{1A}^{*,f}}{\partial n_{1A}^*}\right)\right) \tag{4.9}$$

Similarly, for the second component,

$$\frac{x_{2A}P_A}{x_{2B}P_B} = \exp\left(\frac{1}{RT}\left(\frac{\partial A_{2B}^{*,f}}{\partial n_{2B}^*} - \frac{\partial A_{2A}^{*,f}}{\partial n_{2A}^*}\right)\right) \tag{4.10}$$

In the equations above, the pressure in each layer is expressed through the ideal gas law as,

$$P_A = \frac{\left(n_{1A}^* + n_{2A}^*\right)RT}{V_A} \tag{4.11}$$

$$P_B = \frac{\left(n_{1B}^* + n_{2B}^*\right)RT}{V_B} \tag{4.12}$$

Combining the ideal gas law and chemical potential relations, the following equations are obtained,

$$\frac{n_{1A}^*}{V_A} = \frac{n_{1B}^*}{V_B}\exp\left(\frac{1}{RT}\left(\frac{\partial A_{1B}^{*,f}}{\partial n_{1B}^*} - \frac{\partial A_{1A}^{*,f}}{\partial n_{1A}^*}\right)\right) \tag{4.13}$$

$$\frac{n_{2A}^*}{V_A} = \frac{n_{2B}^*}{V_B}\exp\left(\frac{1}{RT}\left(\frac{\partial A_{2B}^{*,f}}{\partial n_{2B}^*} - \frac{\partial A_{2A}^{*,f}}{\partial n_{2A}^*}\right)\right) \tag{4.14}$$

where the volume of the layers, the temperature, and the field contribution are known, and the unknowns are n^*_{1A}, n^*_{1B}, n^*_{2A}, and n^*_{2B}. Other than equations 4.13 and 4.14, the following two mass balance equations are also used to solve for the four unknowns,

$$n_1 = n^*_{1A} + n^*_{1B} \tag{4.15}$$

$$n_2 = n^*_{2A} + n^*_{2B} \tag{4.16}$$

The initial estimate solution provided by equations 4.13, 4.14, 4.15, and 4.16 is generalized for any number of components or elements in the system. As a result, for the i^{th} component, the solution is,

$$\frac{n^*_{ijm}}{V_{jm}} = \frac{n^*_{i,ref}}{V_{ref}} \exp\left(\frac{1}{RT}\left(\frac{\partial A^{*,f}_{ref}}{\partial n^*_{i,ref}} - \frac{\partial A^{*,f}_{jm}}{\partial n^*_{ijm}}\right)\right) \tag{4.17}$$

$$n_i = \sum_{m=1}^{\hat{r}} \sum_{j=1}^{\ell_m} n^*_{ijm} \tag{4.18}$$

Equation 4.17 is obtained for each layer in the system while considering the layer with the lowest field potential contribution, denoted with the subscript f, as a reference. As a result, for a system with ℓ_m layers, there are $\ell_m - 1$ equations equivalent to equation 4.17. Combined with equation 4.18, the variables, number of moles, are easily found due to the resulting system of equations being linear. This procedure is repeated for each component independently, since the ideal gas law assumes no interactions between the different components in the system. Finally, the amounts of each component are converted to distribution factors in order to serve as a good starting point for the optimization.

4.3 Numerical Considerations

During the optimization process, the resultant distribution factor values at a given iteration, or even at the initial guess stage, might not adhere to some physical constraints dictated by the problem. As a result, while solving the model, the solution vector needs to be checked for any violations. Below is a discussion of the constraints included in the solution method and how these violations are dealt with.

The first technique adopted is to inactivate problematic θ variables. Specifically, in some problems the external potential forces the number of moles in some elements to be very small. Hence, θ variables are checked after generating initial estimates, and after computing a new solution during the optimization. If any variable is found to be below a placed limit ($\theta_{lim} = 1\text{x}10^{-20}$), it is tagged as inactive and is set to zero. Also, tagged variables are not included in the solution vector in the next iteration.

On the other hand, the number of moles in a given element could be very large to the point where they violate the density limit dictated by the EoS used. For any element, the molar volume must be bigger than the b parameter (refer to 3.2.1.1) calculated for that element. To tackle this issue, two molar volume checks are implemented during the calculations. The first check is performed on the ideal gas or initial solution, where for all elements, molar volumes are calculated and compared against b. If violations exist in one variable or more, the amount is set to 1.05 times the value of b and the excess number of moles of each component is calculated. Then, to satisfy mass conservation, the excess moles are distributed among other elements in the system. Rather than adding the number of moles equally to the remaining variables, the excess amount is distributed according to the distribution factor in each element. This is done to avoid disturbance of the molar profile that was initially found.

The second molar volume check is performed during the optimization. Again, after calculating a new set of θ variables, any density violations are looked for. If any variable is found to violate the b parameter limit, the new solution is rejected and the current step size is reduced until high density violations disappear. A similar approach of reducing the step size in the minimization is followed with negative distribution factors, which are meaningless when solving for number of moles.

4.4 Code Development

4.4.1 Use of Thermath Package

To apply the model and the solution method outlined in subsection 4.1, a Fortran program was developed. The program solves for the equilibrium molar distribution given a certain number of regions, layers, or external fields. Besides Fortran, the Thermath package in Mathematica was employed to automatically generate Fortran subroutines that contain properties related to the EoS [54]. In particular, the EoS part of the internal Helmholtz energy expression and its derivatives are derived, starting from the EoS expression. Then, the derived expressions are analyzed and a Fortran subroutine is obtained.

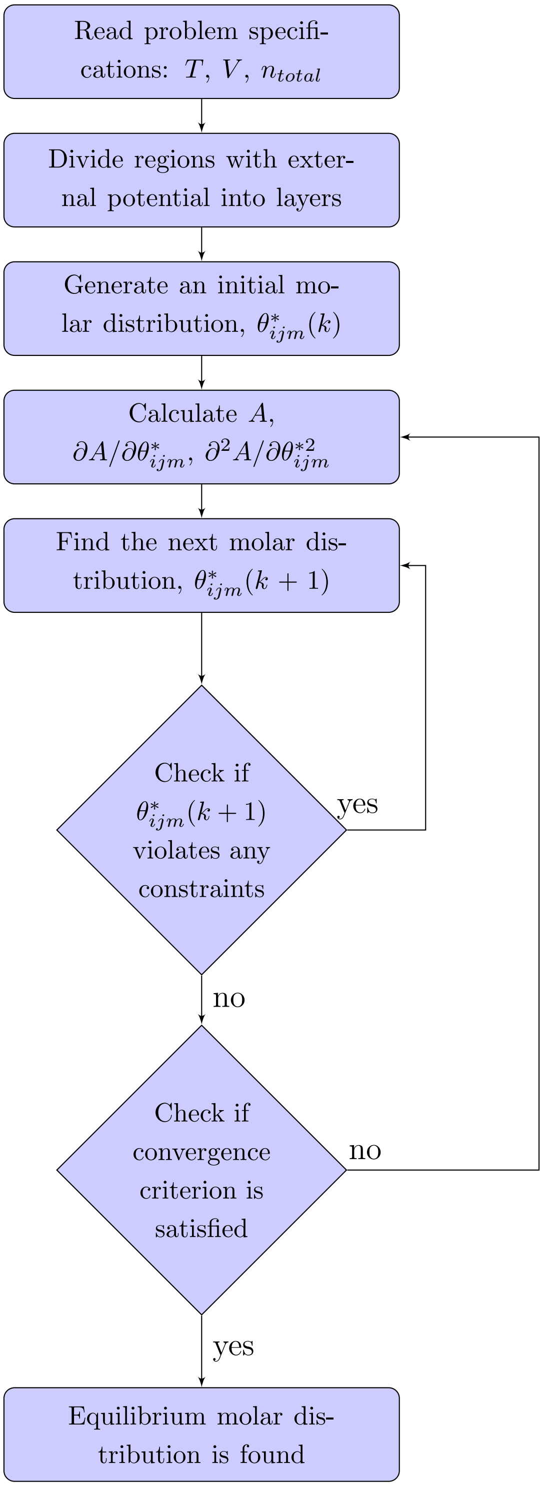

Figure 4.1: Fortran algorithm followed to implement the model solution.

4.4.2 Fortran Algorithm

For the Fortran code, a simplified algorithm for the calculations is presented in Figure 4.1. First, the problem specifications are inputted, which include:

1. T, $\hat{c}$, and n_i.
2. r, volume, and geometry (bulk, slit, cylindrical, or spherical) of each region.
3. For all regions (except bulk regions): direction of external field applied (x, y, z, or r direction), dimensions of the region, and number of layers in the specified direction.
4. The type of potential associated with each direction (Steele potential,...), and its parameters.
5. EoS parameters related to the components of the system, namely, T_c, P_c, ω, k_{ij}, and c.

Based on $\hat{c}$, r, and the maximum number of layers across the regions, the dimensions of many arrays are allocated dynamically, rather than having large arrays with fixed sizes. Dynamic allocation of arrays is advantageous with regard to memory usage.

The next step is to set up the grid in each region with external potentials. This is done based on the spatial dimensions of any region and the number of layers selected. The grid set-up includes calculating the volume of each element in the region, and calculating the coordinates with respect to the directions considered. Also, when applicable, the number of replicas of each region are calculated in this step.

After that, to begin the numerical optimization, an initial molar distribution is computed as discussed previously in subsection 4.2. The linear system of the ideal gas estimate is solved using a L-U decomposition code. The initial molar distribution is checked for any violations related to the nature of the problem (refer to subsection 4.3). Additionally, before the start of the optimization, some parts of the Helmholtz energy and its derivatives are computed. While developing the code, the model equations were broken down to four parts: a part containing constants only, temperature dependent, molar dependent, and molar volume dependent part. For these groups, logical variables were created to control the order in which the parts are computed. Since the temperature is constant throughout the solution, it is possible to compute and save the parts of the model containing temperature and constants before starting the iterative solution procedure.

Next, to start the minimization process, the Helmholtz energy, the gradient vector, and the Hessian matrix are computed using the initial estimate values of the distribution factors. The derivatives are first found with respect to the number of moles in a given layer, and are then converted with respect to the distribution factor as in equations 4.5 and 4.6. After that, the Helmholtz energy and its corresponding derivatives are sent to an optimization routine that computes a new set of variables. The newly calculated variables are then checked for whether they comply with the problem constraints. If they are found to agree, the energy and its derivatives, the gradient and the Hessian, are calculated again to find a new solution vector. The minimization converges to a final equilibrium density distribution when the gradient value is zero.

5. RESULTS AND DISCUSSION

5.1 Adsorption Calculations Details

This subsection includes the numerical values of the parameters required to obtain the results in this section. First, for any component, parameters related to the EoS used are needed. In this work, all EoS parameters have the same value across the system, and no modification or extra parameters are required for confined fluids. For all components studied, Table 5.1 lists PR-EoS parameters, T_c, P_c, and ω [55]. The shift parameter s is obtained from Li et al. [56] where equilibrium liquid density data are fitted.

Table 5.1: PR-EoS parameters for different components [55, 56].

Component	T_c (K)	P_c (MPa)	ω	s
CH_4	190.56	4.599	0.011	-0.1533
C_2H_6	305.32	4.872	0.099	-0.1094
C_3H_8	369.83	4.248	0.153	-0.0869
N_2	126.21	3.796	0.039	-0.16562
CO_2	304.14	3.37	0.239	-0.06225

Next, the for the confined regions in the system, parameters related to the adsorption potential are provided. In the case of using the Steele potential the parameters are taken from Li et al. [56] and included in Table 5.2. For calculations that utilize the DRA potential, the parameters characterizing the system considered are: $v_o = 4.093$ x 10^{-4} m^3/kg, and the characteristic energies are 8143 J/mol, 7980 J/mol, and 6.328 J/mol for CH_4, CO_2, and N_2 respectively. The parameters were fitted to pure components adsorption by Monsalvo and Shapiro using the DRA-SRK version of their MPTA model [40].

Table 5.2: Steele potential parameters: energy parameter for each component and solid related parameters [56].

Fluid parameters		Solid parameters	
components	ε_i/k_B (K)	ε_s/k_B (K)	20
CH_4	1178	σ_s (m)	3.345x10^{-10}
CO_2	1760	δ (m)	3.35x10^{-10}
C_3H_8	1866	ρ_s (m^{-3})	1.14x10^{29}

Other than the parameters related to the components and solid investigated, the framework requires no other information for regions subject to confinement. In this work, the confinement in activated carbon pores was studied. For this porous medium, slit shape is assumed and the geometry of the confined region is selected to be rectangular. For this geometry, the pore width, H is provided as well as details on the discretization of the confined region. Namely, the number of layers perpendicular to the solid wall is specified. This is determined by increasing the number of layers until grid convergence is achieved, or increasing the number the number of layers is no longer affecting the solution obtained. For the adsorption calculations performed in this work, 100 layers were found sufficient.

Finally, the methodology proposed in this work requires specification of the temperature, bulk and pore volumes, and total amount of each component ($TV\underline{N}$). Once the Helmholtz energy is minimized at these specifications, the density and composition in each region is obtained along with the bulk pressure. However, sometimes it is desired to obtain the density at a specific bulk phase pressure, temperature and bulk composition, for example, to compare with adsorption data reported at these conditions. In such cases, the number of moles is varied until the desired conditions are obtained.

5.2 Steele Potential Results

5.2.1 Adsorption in a Single Slit Pore

The local density profiles of CH_4 inside an activated carbon pore with a pore width of 2.0 nm at various pressures and $T = 298\ K$ is depicted in Fig. 5.1. The plot highlights a few features of adsorption in slit pores at the given pressure range. Since both walls are characterized using the same energy, the density distribution is symmetric, with most of the adsorbed fluid accumulated near the pore walls due to the maximum potential effect experienced there. Moving away from the wall and towards the center of the pore, the solid-fluid interactions become weaker as fluid-fluid interactions begin to dominate. Less amounts are adsorbed, until a near-constant density is reached in the middle of the pore. Another important observation is related to the effect of the bulk pressure on the density profile. As the pressure increases, the amounts inside the pore are expected to increase, with higher pressures corresponding to higher density maxima. Once the density of each layer in the pore is calculated, the density of each component in the confined region m is obtained, which is defined as,

$$\rho_{im} = \frac{1}{H_{in}} \int_0^H \rho_{im}(z_m) dz_m \tag{5.1}$$

where H_{in} is the internal pore width (excluding the radius of the adsorbent molecule). Using numerical discretization, the adsorbed amount is calculated by adding the number of moles at each distance and dividing by the pore volume in region m (V_m), according to,

$$\rho_{im} = \frac{H}{H_{in}} \frac{\sum_{j=1}^{lm} n^*_{ijm}}{V_m} \tag{5.2}$$

where the factor H/H_{in} is used to obtain the density within the effective pore volume.

As soon as the calculations converge, the pressure in the bulk region is computed. Fig. 5.2 shows the adsorption of CH_4 reported for wall-to-wall distances of 2, 3 and 6 nm respectively, for a pressure range of $0-30\ MPa$. The results are plotted along with the DFT results obtained by Li et al. In general, the model perform well when compared with the DFT calculations, especially in the high pressure range (above 5 MPa). Additionally, the plots demonstrate the effect of pore size on the amounts adsorbed. As the pore width decreases, the density at a given pressure increases.

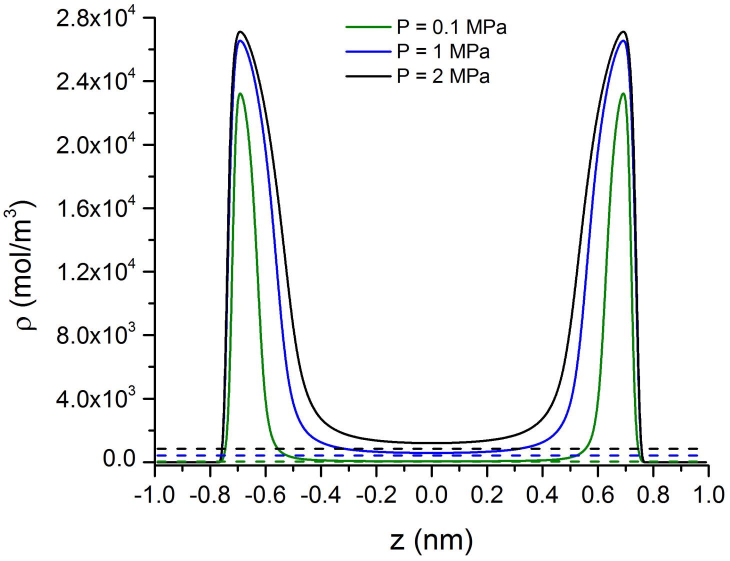

Figure 5.1: Local density profiles for CH_4 at T= 298 K and H= 2nm using the parameters in Table 5.2.

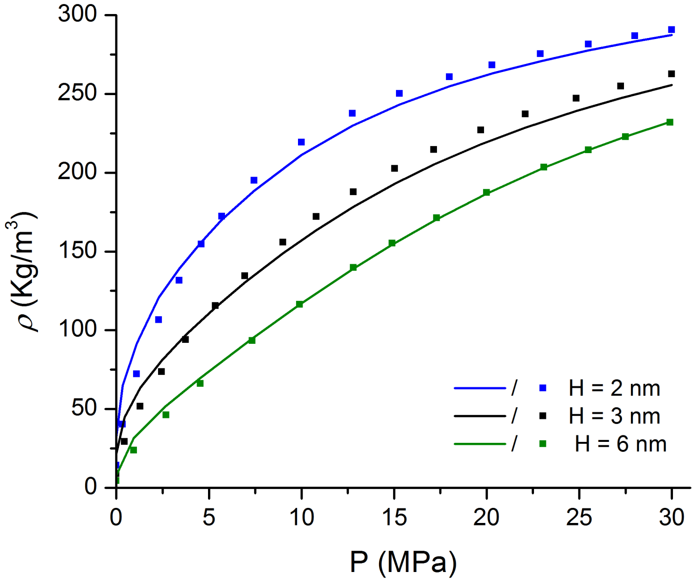

Figure 5.2: CH_4 adsorption isotherm at T =303.15 K for various pore widths. Solid lines represent predictions of this work, while the points are predictions by a DFT model [56].

The model is also capable of predicting the compositional profiles inside the pore for binary mixtures. In Fig. 5.3, an equimolar mixture of CH_4 and C_3H_8 is studied in a pore width of 10 nm at 323.15 K and 0.5 MPa, with the Steele potential parameters taken from Table 5.2. The mole fraction of both components is plotted against distance. The compositional profile is symmetric, and only the wall-to-center distance is shown. Based on the energy parameters listed in Table 5.2, it can be deduced that propane will be more favorably attracted to the solid wall than CH_4. However, the plot depicts that the first molecular layer formed next to the wall is made up of pure CH_4 and after that, pure C_3H_8 is adsorbed. The packing order observed inside the pore is due to CH_4 having a smaller molecular diameter than C_3H_8. Setting the energy parameters for both components to be equal, while keeping the size difference, will result in a similar local compositional profiles. In the middle of the pore, the adsorption effect is not as pronounced, and equal amounts of each component are present, similar to bulk conditions. Also, the compositional profile for the same mixture, predicted by the DFT model is shown. The two models, although following two different methods, agree qualitatively.

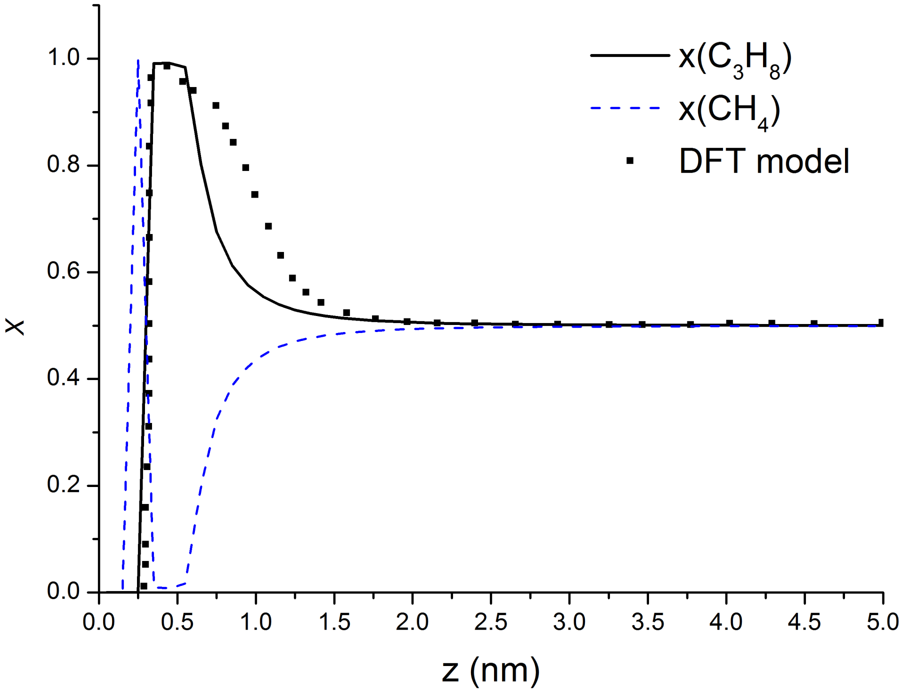

Figure 5.3: Compositional profiles for mixture of C1/C3 at T= 323.15 K, P=5 bar, equimolar bulk, and H= 10 nm. DFT predictions are from Li et al. [56].

5.2.2 Adsorption in Multiples Slit Pores

The work by Li et al. [56] use their DFT model to characterize the pore size distribution (PSD) of a certain activated carbon sample through using experimental data provided by Qiao et al. [57]. For adsorbents comprised of pores with different sizes, the PSD provides the volume for each pore size. In this work, the PSD results of Li et al. [56] are used calculate the adsorption of CH_4 in the heterogeneous solid with multiple pore widths.

To simplify the calculations, pores with negligible volumes are discarded. Table 5.3 presents the PSD values for the pores considered. This PSD is used to obtain the pore volume, $V_m(H_m)$, of region m with specific pore width H_m using the following relation,

$$V_m(H_m) = \frac{1}{2}\frac{PSD(H_m) + PSD(H_{m+1})}{H_{m+1} - H_m} \tag{5.3}$$

Table 5.3: Pore size distribution and pore volumes.

H_m	$PSD(H_m)$	V_m
nm	$m^3/kg/nm$	m^3/kg
0.8	3.030E-06	3.818E-06
0.9	7.333E-05	2.381E-05
1	4.029E-04	6.341E-05
1.1	8.653E-04	9.289E-05
1.2	9.925E-04	8.649E-05
1.3	7.373E-04	5.697E-05
1.4	4.020E-04	2.886E-05
1.5	1.751E-04	1.199E-05
1.6	6.462E-05	4.286E-06
1.7	2.109E-05	1.369E-06
1.8	6.280E-06	4.010E-07

Having obtained this information, the amount adsorbed in each pore is found at a specific bulk pressure. Then to find the total adsorbed amount of a pure component, the following relation is used,

$$N_{ads} = \sum_{m=1}^{\hat{r}_{conf}} \rho_m V_m(H_m) \tag{5.4}$$

where $\hat{r}_{conf}$ is the number of confined regions. Finally, the adsorption isotherm of CH_4 within a pressure range of $0.01 - 0.11$ MPa at 363 K was computed. These are then compared to the experimental data and the DFT results. When using the reported DFT Steele energy parameters to perform calculations, there is significant deviation observed between the experimental data, and model predictions of CH_4 in Fig. 5.4. To reduce the deviations, the energy parameter in the Steele potential was modified. As depicted in Fig. 5.4, it was found that by using a value of 865 K for ε/k_B the predictions of the model is enhanced and deviations between experimental data and calculations are minimized.

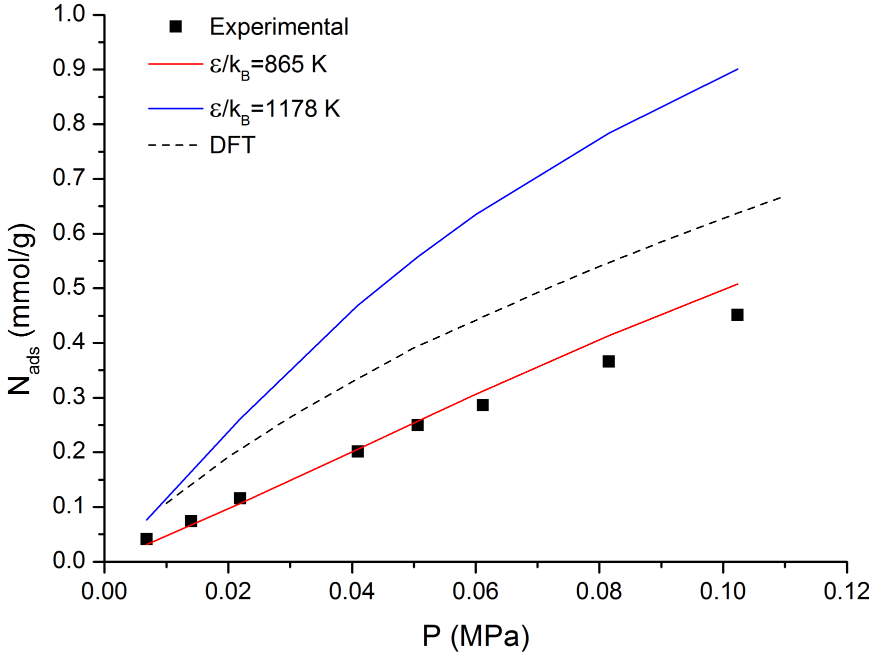

Figure 5.4: CH_4 adsorption isotherm at $T = 363.15\ K$ at $\varepsilon = 865\ K$ and $1178\ K$. Lines represent predictions of this work, points are experimental data [57] and the dashed line represent DFT calculations [56].

5.3 DRA Potential Results

In this subsection, calculations are performed for CH_4, CO_2, and N_2, and their mixtures adsorbed on activated carbon using the DRA potential. The predictions are compared with experimental data from Dreisbach et al. [58], and the same data are used by Monsalvo and Shapiro [40] to fit the pure component parameters for this system. From their DRA-SRK model, the following parameters were found: $v_o = 4.093 \text{ x } 10^{-4} m^3/kg$, and the characteristic energies are 8143 J/mol, 7980 J/mol, and 6.328 J/mol for CH_4, CO_2, and N_2 respectively. These parameters were used in this work to model the studied system with no additional parameters needed for mixtures. As in the previous example, volume translation was applied to the PR EoS to obtain better results.

For adsorption data, the surface excess is usually measured and reported at a given temperature and pressure. The surface excess in region m, Γ_{im}, of each component is computed by subtracting the bulk amount from the adsorbed amount,

$$\Gamma_{im} = \frac{V_m}{H} \int_0^H (\rho(z)x_i(z) - \rho_B x_{Bi})dz \tag{5.5}$$

In this work, equation 5.5 is simplified to,

$$\Gamma_{im} = (\sum_{j=1}^{lm} n^*_{ijm}) - V_m \rho_B x_{Bi} \tag{5.6}$$

The individual excess amounts are added to find the total surface excess, Γ_m. Subsequently, the mole fraction of the i^{th} component in the adsorbate is:

$$x_{ex,im} = \frac{\Gamma_{im}}{\Gamma_m} = \frac{\Gamma_{im}}{\sum\limits_{j=1}^{\hat{c}} \Gamma_{jm}} \tag{5.7}$$

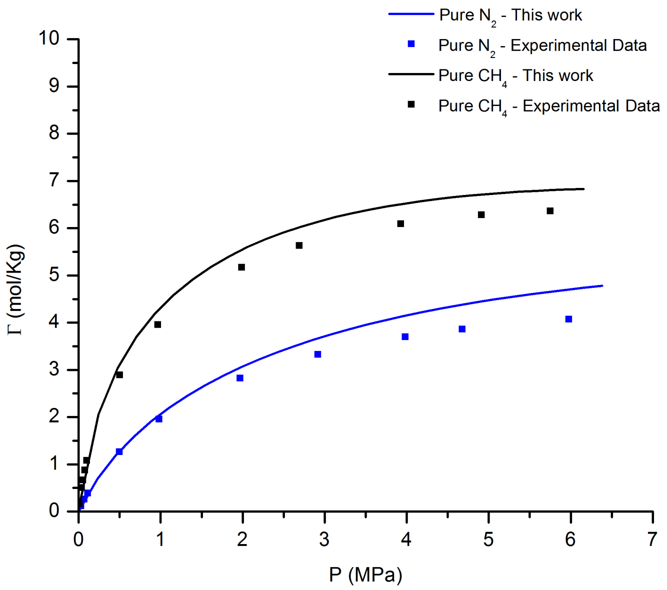

Figure 5.5: Surface excess values for the adsorption of pure N_2 and CH_4 on activated carbon at T = 298 K. Solid lines are predictions by this work and points are experimental data [58].

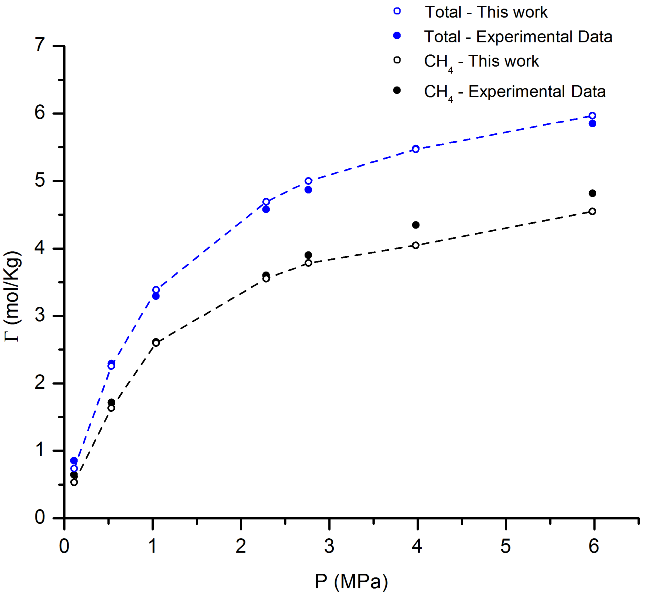

Figure 5.6: Adsorption of CH_4 and N_2 mixture at T = 298 K and $x_{B,CH_4} = 0.4$. Empty symbols are predictions by this work and filled symbols are experimental data [58]. Dashed lines are linear interpolations between calculations.

The deviation between experimental data and calculations for each data point is computed, and the average deviation in Γ, N_{ads}, and $x_{ex,im}$ for each mixture (for $\hat{p}$ data points) is computed according to the following relations,

$$ADD_{\Gamma}(\%) = \frac{100}{\hat{p}} \sum_{i=1}^{\hat{p}} \left| (\Gamma^{\exp,i} - \Gamma^{calc,im}) / \Gamma^{\exp,i} \right| \tag{5.8}$$

$$ADD_{N_{ads}}(\%) = \frac{100}{\hat{p}} \sum_{i=1}^{\hat{p}} \left| (N_{ads}^{\exp,i} - N_{ads}^{calc,i}) / N_{ads}^{\exp,i} \right| \tag{5.9}$$

$$ADD_{x}(\%) = \frac{100}{\hat{p}} \sum_{i=1}^{\hat{p}} \left| x_{ex,i}^{\exp} - x_{ex,im}^{calc} \right| \tag{5.10}$$

In Fig. 5.5, the surface excess predictions for pure CH_4 and N_2 are reported for a temperature of 298 K and pressures up to 6 MPa. Overall, the model captures reasonably well the type of adsorption isotherm of each component. Further, accurate predictions for these two components are obtained at low pressures. Then, as the bulk pressure increases, the deviations from experimental data increase for both components.

Next, the total and individual surface excess values were computed at the same temperature and pressure range for binary and ternary mixtures. The experimental data for these mixtures were reported at different bulk compositions and the calculations were done at the exact reported compositions to obtain an accurate comparison. Fig. 5.6, 5.7, and 5.8 show the results for the binary mixtures of CH_4-N_2, CH_4-CO_2, and CO_2-N_2 respectively. Also, Fig. 5.9 shows the results for the ternary mixture of $CH_4 - CO_2 - N_2$. In all figures, the closed symbols represent experimental data, open symbols represent model calculations, and dashed lines are interpolations between the calculated values. In general, more satisfactory results are obtained at low pressures, as in the case of pure components. The adsorption of CH_4 is more accurately predicted over the entire pressure range, while relatively larger deviations are experienced in the cases of N_2 and CO_2. For instance, the highest average deviation value is reported for $CO_2 - N_2$ mixture. Table 5.4 lists the deviations between this work and experimental data for all the computed points of various compositions.The results for all conditions for and mixtures are provided in Appendix A.

Furthermore, the $ADD_{x_{ex,i}}$, and $ADD_{N_{ads}}$ values obtained by Monsalvo and Shapiro [40] are included for comparison. The error values reported in the table are relatively small, considering the few parameters required. Good performance is especially observed with respect to the adsorbed compositions values (maximum $ADD_{x_{ex,i}}$ is 8.7%). Monsalvo and Shapiro [40] suggest that the results could be enhanced by determining the adsorptive capacities of each component, rather than finding one common capacity for all components. Likewise, the effect of other parameters on the model performance could be further investigated. That includes the heterogeneity parameter in the DRA potential, and the binary interaction parameter in the EoS.

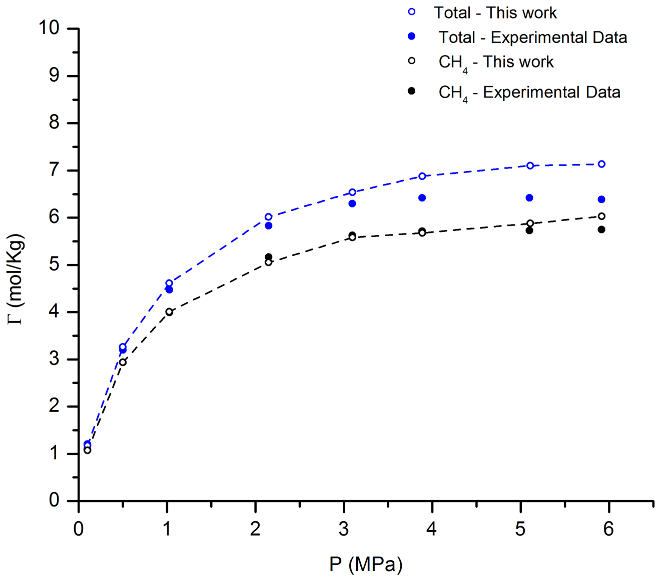

Figure 5.7: Adsorption of CH_4 and CO_2 mixture at T = 298 K and $x_{B,CH_4} = 0.9$.

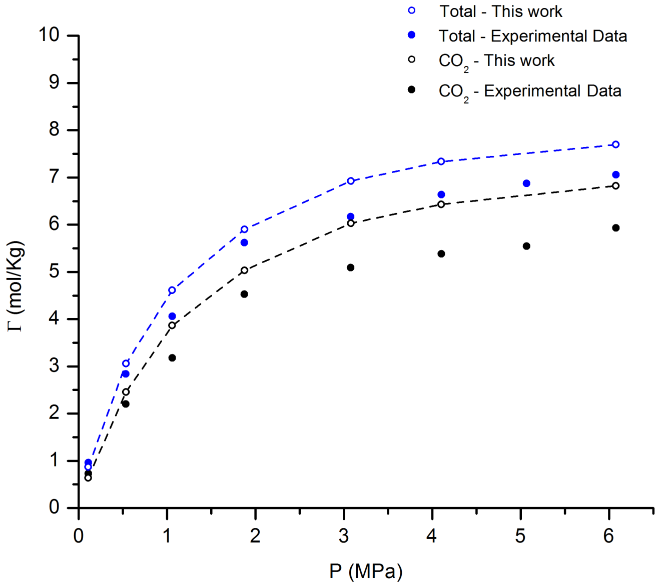

Figure 5.8: Adsorption of CO_2 and N_2 mixture at T = 298 K and $x_{B,CO_2} = 0.2$.

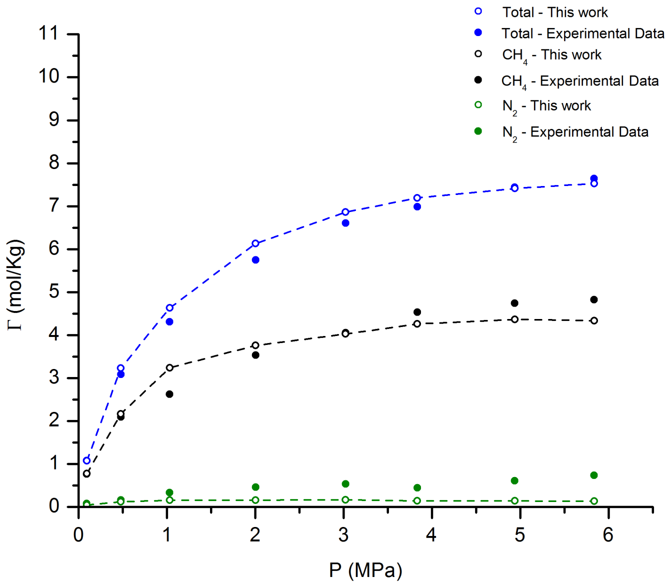

Figure 5.9: Adsorption of CH_4, CO_2 and N_2 mixture at T = 298 K, $x_{B,CH_4} = 0.7$ and $x_{B,CO_2} = 0.1$.

Table 5.4: Average deviations for binary and ternary mixtures using DRA potential.

Mixture	Γ Total surface excess (%)	$x_{ex,i}$ Mole fraction in the adsorbate (%)		N_{ads} Absolute adsorbed amount (%)	
	This work	*This work*	*MPTA*	*This work*	*MPTA*
$CH_4 - N_2$	6.08	3.38	2.52	10.5	4.45
$CH_4 - CO_2$	5.32	3.94	4.20	7.66	7.39
$CO_2 - N_2$	9.55	4.18	3.75	11.8	7.89
$CH_4 - CO_2 - N_2$	5.93	8.70	17.5	6.70	9.38

5.4 Results for Multiple Fields

The equilibrium molar distribution of a mixture of 80% mol CH_4 and 20% mol CO_2 is obtained for a reservoir depth of 4000 m at $T = 305\ K$. Steele potential was used to describe confinement in an activated carbon pore with $H = 6\ nm$. Using this potential enables the prediction of the amount adsorbed or the density inside the pore, as well as distribution of components in porous media. The gravitational field effect, which is assumed to act on a system consisting of a bulk phase and a slit pore is included in the equilibrium calculations.

The variations in the amount adsorbed with respect to depth can be correlated to the variation of bulk pressure with depth. The pressure profile is presented in Figure 5.10, while Figure 5.11 show the variations of density in the porous space with depth. Overall, CH_4 is more adsorbed and has higher molar concentrations throughout the reservoir column. Also, the amount adsorbed increases with depth for both components, but differently. For CO_2, the change in the adsorbed amount is greater due to the fact that CO_2 has a larger molecular weight and thus is more affected by gravitational effects.

Figure 5.12 shows the compositional profile of CO_2 at $h = -200\ m$ and $h = -3800\ m$. For all heights, CO_2 has high mole fraction near the solid wall, although the bulk composition and total amount adsorbed for CH_4 is higher. This could be explained by the higher energy parameters for CO_2 used (refer to 5.1), which results in its molecules being much more present near the wall, where adsorption potential is the strongest. Moving away from the wall, the mole fraction of CO_2 starts decreasing until reaching a near-constant value at the center of the pore ($H = 3\ nm$). Moreover, gravitational effects have an impact on local density profiles inside the slit pores studied. Namely, various depths correspond to different amounts adsorbed near the

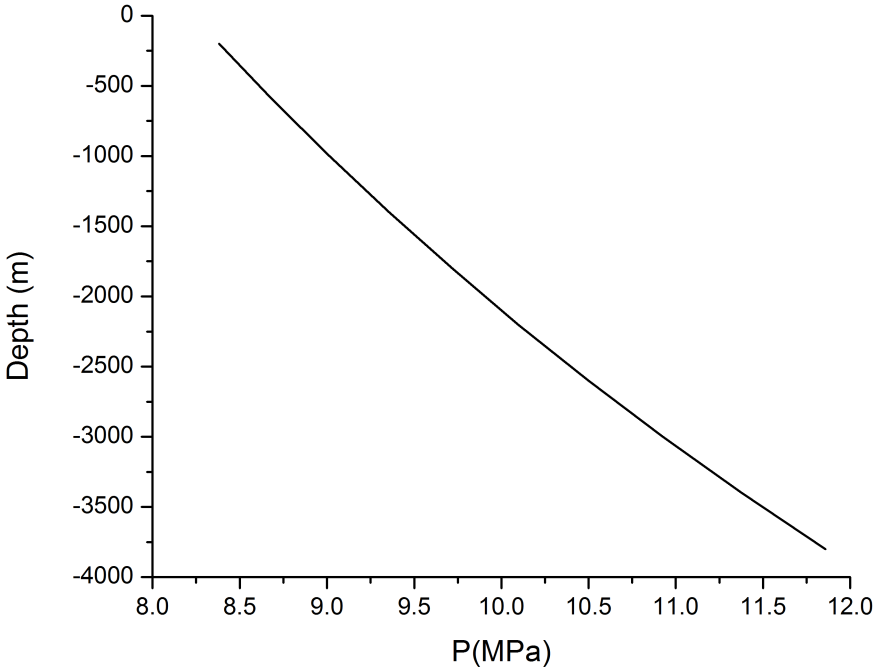

Figure 5.10: Bulk pressure profile with depth at $T = 330\ K$.

wall. Figure 5.12 shows with increasing the depth, the maximum amount adsorbed near the wall increases as well as the mole fraction in the center of the pore.

Finally, some remarks could be made regarding the computational performance of the framework. In this case, to accurately model both effects, the confined region was divided to 500 grids. This number of elements corresponds to 1000 variables (500 per component). Calculations for this number of variables take about 4 minutes of CPU time in a Lenovo laptop model Yoga2015 (equipped with an Intel processor model $i7-4500U$ and a 8 GB memory). This the highest amount of time reported in this work. Other calculations involving only confinement converge within around 60 seconds. As a result, measures to reduce the computational requirements of this model should be considered.

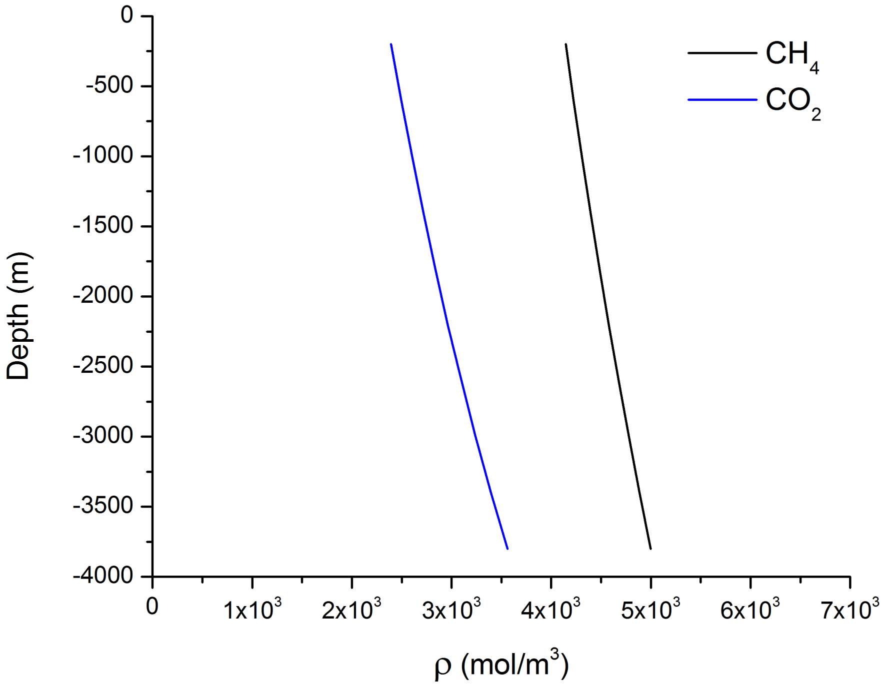

Figure 5.11: Density distribution with depth for CH_4 and CO_2, inside a slit pore.

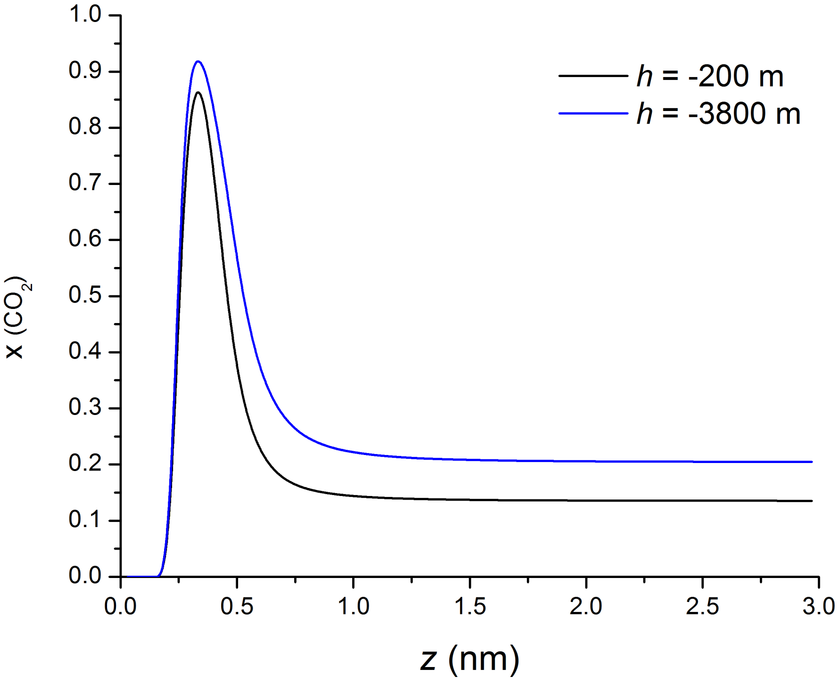

Figure 5.12: Local compositional profiles for CO_2 at $h = -200m$ and $h = -3800m$.

6. CONCLUSIONS

In this work, a thermodynamic model was developed to study confinement. By specifying the temperature, total amount and total volume, the distribution of the components in the confined and bulk regions is computed. The equilibrium density distribution is found by minimizing the Helmholtz energy, which accounts for the effect of adsorption through an appropriate potential. Additionally, to account for internal interactions, the volume translated PR-EoS was used to model all the components studied. The theoretical model was then solved numerically using a general computer code that was developed to be applied for many types of adsorption calculations.

The performance of the framework was tested by applying the Steele and DRA potentials for adsorption in activated carbon. The Steele potential proved adequate in describing local density and compositional profiles of the studied systems. The model performance was validated by comparing the results with the predictions of a model based on DFT, proposed by Li et al. The local density profiles predicted in this work were found comparable to those computed using DFT. Additionally, the Steele potential was used to obtain adsorption isotherms. Good agreement between experimental data and calculations was obtained after using a modified energy parameter.

Reasonable agreement between the model calculations and experimental data for the adsorption of CH_4, CO_2, and N_2 was obtained when applying the DRA potential. The average deviations for the binary and ternary mixtures are comparable to those obtained using an MPTA model. Once again, investigating the effect of various parameters could lead to more accurate predictions for modeling the effect of confinement. However, such modifications might include an increase in the number of fitted parameters, thus complicating the overall approach. Finally, the proposed methodology was applied for the case of having other fields, besides adsorption potential. In the case of fluids exposed to multiple external effects (confinement and gravity), it was determined that the local density within the pore is influenced by the presence of both effects.

7. FUTURE WORK

In this thesis, a framework for determining equilibrium conditions in systems including confined fluids was established. Furthermore, the methodology was extended to account for effects other than confinement. Based on the general approach developed and findings of this work there are many possible directions for future work.

First, for the current adsorption systems studied, better results could be obtained through fitting parameters in the adsorption models to experimental data. Moreover, including routines to minimize the error between experimental data and the calculations of this work will allow for studying any system, without requiring parameters from other models found in literature. Second, a phase stability test could be implemented in the framework to study systems with multiple phases. As a result, phase behavior of fluids under confinement could be investigated. This is relevant to many applications, including locating oil-water contact zones in reservoirs. Other than phase equilibria calculations, the framework could be extended to involve chemical equilibrium calculations. That would require including the formation properties of various components to the energy of the system. Such computations are useful for processes involving heterogeneous catalysis. While the addition of extra features will lead to the computation time increase, there are some possibilities for optimizing the computer codes used in solving the model. Namely, when predicting symmetric density profiles, only half of the profile could be computed, thus reducing the number of variables significantly. Additionally, for the same type of problem, it is more important to solve for amount adsorbed close to the solid wall, where the adsorption potential is stronger. Currently, all layers have the same volume everywhere in the pore. However, it is possible to use multiple grid sizes within a pore.

So far, this work has studied confinement in slit pores only, which is useful to many applications related to the oil and gas industry. Nonetheless, there is a wide range of porous solids utilized in industry that could be modeled as spherical or cylindrical pores. To perform equilibrium calculations with such geometries, implementing the appropriate adsorption potentials is required. Moreover, the methodology is established to deal with problems where more than one geometry, or one size, could be present in one adsorbent. Another advantage of this framework, is the ability to combine these microscopic effects with external fields at larger scale. While the ability of the framework to predict adsorption when a gravitational field is acting was demonstrated, other effects could be modeled including centrifugal field and electrical field. Finally, another direction that would increase the number of applications considered is to use other EoS models. For instance a Statistical Associating Fluid Theory EoS could be implemented to represent polar or associating systems.

REFERENCES

[1] P. Charoensuppanimit, S. A. Mohammad, R. L. Robinson, and K. A.M. Gasem, "Modeling the temperature dependence of supercritical gas adsorption on activated carbons, coals and shales," *International Journal of Coal Geology*, vol. 138, pp. 113–126, 2015.

[2] R. T. Yang, *Adsorbents Fundamentals and Applications.* New Jersey: Wiley Interscience, 2003.

[3] L. Zhou, *Adsorption: Progress in Fundamental and Application Research.* World Scientific Publishing, 2006.

[4] D. D. Do, *Adsorption Analysis: Equilibria and Kinetics.* London: Imperial College Press, 1998.

[5] R. T. Yang, *Gas Separation by Adsorption Processes.* London: Imperial College Press, 1997.

[6] D. Ruthven, *Principles of Adsorption & Adsorption Processes.* New York: Wiley Interscience, 1984.

[7] L. Travalloni, M. Castier, F. W. Tavares, and S. I. Sandler, "Critical behavior of pure confined fluids from an extension of the van der Waals equation of state," *Journal of Supercritical Fluids*, vol. 55, pp. 455–461, 2010.

[8] G. J. Zarragoicoechea and V. A. Kuz, "van der Waals equation of state for a fluid in a nanopore," *Physical Review E*, vol. 65, pp. 1–4, 2002.

[9] I. Langmuir, “The Adsorption of Gases on Plane Surfaces of Glass, Mica and Platinum,” *Journal of the American Chemical Society*, vol. 40, no. 9, pp. 1361–1403, 1918.

[10] J. Toth, “Uniform Interpretation of Gas/Soild Adsorption,” *Advances in Colloid and Interface Science*, vol. 55, pp. 1–239, 1995.

[11] R. Sips, “On the Structure of a Catalyst Surface. II,” *The Journal of Chemical Physics*, vol. 18, no. 1948, p. 1024, 1950.

[12] D. N. Misra, “Jovanovich adsorption isotherm for heterogeneous surfaces,” *Journal of Colloid And Interface Science*, vol. 43, no. 1, pp. 85–88, 1973.

[13] S. Brunauer, P. H. Emmett, and E. Teller, “Adsorption of Gases in Multimolecular Layers,” *Journal of the American Chemical Society*, vol. 60, no. 2, pp. 309–319, 1938.

[14] J. C. Melrose, “Model Calculations for Capillary Condensation,” *AIChE Journal*, vol. 12, no. 5, pp. 986–994, 1966.

[15] M. M. Dubinin and V. A. Astakhov, “Adsorbents, Development of the Concept of Volume Filling of Micropores in the Adsorption of Gases and Vapors by Microporous Adsorbents,” *Physical Chemistry*, vol. 1, pp. 5 – 11, 1971.

[16] M. M. Dubinin, “Generalization of the Theory of Volume Filling of Micropores to Nonhomogeneous Microporous Structure,” *Carbon*, vol. 23, no. 4, pp. 373–380, 1985.

[17] A. L. Myers and J. M. Prausnitz, “Thermodynamics of mixed-gas adsorption,” *AIChE Journal*, vol. 11, no. 1, pp. 121–127, 1965.

[18] C. J. Radke and J. M. Prausnitz, “Thermodynamics of Multi-Solute Adsorption from Dilute Liquid Solutions,” *AIChE Journal*, vol. 18, no. 4, pp. 761–768, 1972.

[19] W. Fritz and E. U. Schlonder, “Competitive Adsorption of Two Dissolved Organics onto Activated Carbon - I,” *Chemical Engineering Science*, vol. 36, pp. 721–730, 1981.

[20] M. Okazaki, H. Kage, and R. Toei, “Prediction Equilibria of Liquid Phase Adsorption of Multi-solutes in Water,” *Journal of Chemical Engineering of Japan*, vol. 13, no. 4, pp. 286–291, 1980.

[21] L. Jossens, J. M. Prausnitz, W. Fritz, E. U. Schlunder, and a. L. Myers, “Thermodynamics of Multi-solute Adsorption from Dilute Aqueous Solutions,” *Chemical Engineering Science*, vol. 33, pp. 1097–1106, 1978.

[22] A. L. Myers, “Activity coefficients of mixtures adsorbed on heterogeneous surfaces,” *AIChE Journal*, vol. 29, no. 4, pp. 691–693, 1983.

[23] E. Costa, G. Calleja, C. Marron, A. Jimenez, and J. Pau, “Equilibrium Adsorption of Methane, Ethane, Ethylne, and Propylene and Thier Mixtures on Activated Carbon,” *Journal of Chemical Engineering Data*, vol. 34, no. 2, pp. 156–160, 1989.

[24] S. Sochard and N. Fernandes, “Modeling of Adsorption Isotherm of a Binary Mixture with Real Adsorbed Solution Theory and Nonrandom Two-Liquid Model,” *AIChE Journal*, vol. 56, no. 12, pp. 3109–3119, 2010.

[25] M. G. Bjørner, E. Solbraa, A. Shapiro, and G. M. Kontogeorgis, “Capabilities and Limitations of Predictive Engineering Theories for Multicomponent Adsorp-

tion," *Industrial & Engineering Chemistry Research*, vol. 52, pp. 11552–11563, 2013.

[26] R. Evans, U. M. B. Marconi, and P. Tarazona, "Fluids in narrow pores: Adsorption, capillary condensation, and critical points.," *Journal of Chemical Physics*, vol. 84, no. 4, pp. 2376–2399, 1985.

[27] T. F. Meister and D. M. Kroll, "Density-functional theory for inhomogeneous fluids: Application to wetting," *Physical Review A*, vol. 31, no. 6, pp. 4055–4057, 1985.

[28] T. Vanderlick, L. Scriven, and H. Davis, "Molecular theories of confined fluids.," *Journal of Chemical Physics*, vol. 90, no. 4, pp. 2422 – 2436, 1988.

[29] E. Kierlik and M. Rosinberg, "Density-functional theory for inhomogeneous fluids: Adsorption of binary mixtures," *Physical Review A*, vol. 44, no. 8, pp. 5025–5037, 1991.

[30] J. Wu and Z. Li, "Density-Functional Theory for Complex Fluids," *Annual Review of Physical Chemistry*, vol. 58, pp. 85–112, 2007.

[31] M. W. Maddox, J. P. Olivier, and K. E. Gubbins, "Characterization of MCM-41 Using Molecular Simulation : Heterogeneity Effects," *Langmuir*, vol. 7463, no. 6, pp. 1737–1745, 1997.

[32] V. Y. Gusev, J. A. O. Brien, and N. A. Seaton, "A Self-Consistent Method for Characterization of Activated Carbons Using Supercritical Adsorption and Grand Canonical Monte Carlo Simulations," *Langmuir*, vol. 7463, no. November 1995, pp. 2815–2821, 1997.

[33] M. B. Sweatman and N. Quirke, "Modelling Gas Adsorption in Slit-Pores Using Monte Carlo Simulation," *Molecular Simulation*, vol. 27, pp. 295–321, nov 2001.

[34] B. L. Severson and R. Q. Snurr, "Monte Carlo simulation of n-alkane adsorption isotherms in carbon slit pores.," *The Journal of Chemical Physics*, vol. 126, p. 134708, apr 2007.

[35] Y. Hamada, K. Koga, and H. Tanaka, "Phase behavior and fluidsolid surface tension of argon in slit pores and carbon nanotubes," *Physica A: Statistical Mechanics and its Applications*, vol. 388, pp. 2289–2298, jun 2009.

[36] L. D. Gelb, K. E. Gubbins, R. Radhakrishnan, and M. Sliwinska-Bartkowiak, "Phase separation in confined systems," *Reports on Progress in Physics*, vol. 62, pp. 1573–1659, 1999.

[37] A. A. Shapiro and E. H. Stenby, "Potential Theory of Multicomponent Adsorption," *Journal of Colloid and Interface Science*, vol. 201, pp. 146–157, may 1998.

[38] M. Polanyi, "Theories of the adsorption of gases. A general survey and some additional remarks.," *Transactions of the Faraday Society*, vol. 28, pp. 316–333, 1932.

[39] M. A. Monsalvo and A. A. Shapiro, "Study of high-pressure adsorption from supercritical fluids by the potential theory," *Fluid Phase Equilibria*, vol. 283, pp. 56–64, sep 2009.

[40] M. A. Monsalvo and A. A. Shapiro, "Modeling adsorption of binary and ternary mixtures on microporous media," *Fluid Phase Equilibria*, vol. 254, no. 1-2, pp. 91–100, 2007.

[41] E. Dundar, R. Zacharia, R. Chahine, and P. Bénard, "Modified potential theory for modeling supercritical gas adsorption," *International Journal of Hydrogen Energy*, vol. 37, pp. 9137–9147, 2012.

[42] E. Dundar, R. Zacharia, R. Chahine, and P. Bénard, "Potential theory for prediction of high-pressure gas mixture adsorption on activated carbon and MOFs," *Separation and Purification Technology*, vol. 135, pp. 229–242, 2014.

[43] L. Travalloni, M. Castier, F. W. Tavares, and S. I. Sandler, "Thermodynamic modeling of confined fluids using an extension of the generalized van der Waals theory," *Chemical Engineering Science*, vol. 65, pp. 3088–3099, 2010.

[44] L. Travalloni, M. Castier, and F. W. Tavares, "Phase equilibrium of fluids confined in porous media from an extended Peng Robinson equation of state," *Fluid Phase Equilibria*, vol. 362, pp. 335–341, 2014.

[45] A. W. Islam, T. W. Patzek, and A. Y. Sun, "Thermodynamics phase changes of nanopore fluids," *Journal of Natural Gas Science and Engineering*, vol. 25, pp. 134–139, 2015.

[46] S. P. Tan and M. Piri, "Equation-of-state modeling of confined-fluid phase equilibria in nanopores," *Fluid Phase Equilibria*, vol. 393, pp. 48–63, 2015.

[47] M. L. Michelsen and J. M. Mollerup, *Thermodynamic Models: Fundamentals & Computational Aspects*. Holte: Tie-Line Publications, second ed., 2007.

[48] D. Y. Peng and D. B. Robinson, "A New Two-Constant Equation of State," *Industrial & Engineering Chemistry Fundamentals*, vol. 15, no. 1, pp. 59–64, 1976.

[49] D. B. Robinson, D. Y. Peng, and S. Chung, "The Development of The Peng - Robinson Equation and its Application of Phase Equilibrium in a System Containing Methanol," *Fluid Phase Equilibria*, vol. 24, pp. 25–41, 1985.

[50] B. S. Jhaverl and G. K. Youngren, "Three-Parameter Modification of the Peng-Robinson Equation of State To Improve Volumetric Predictions," *SPE Reservoir Engineering*, pp. 1033–1040, 1998.

[51] W. A. Steele, "The Physical Interaction of Gases with Crystalline Solids I. Gas-Solid Energies and Properties of Isolated Adsorbed Atoms," *Surface Science*, vol. 36, pp. 317–352, 1973.

[52] S. I. Sandler, *An Introduction to Applied Statistical Thermodynamics.* Wiley & Sons, 2011.

[53] W. Murray, "Second Derivative Methods," in *Numerical Methods for Unconstrained Optimization*, pp. 57–71, London: Academic Press, 1972.

[54] M. Castier, "Automatic implementation of thermodynamic models using computer algebra," *Computer & Chemical Engineering*, vol. 23, pp. 1229–1245, 1999.

[55] B. E. Poling and J. M. Prausnitz, *The Properties of Gases and Liquids.* New York: McGraw Hill, 5 ed., 2001.

[56] Z. Li, Z. Jin, and A. Firoozabadi, "Phase Behavior and Adsorption of Pure Substances and Mixtures and Characterization in Nanopore Structures by Density Functional Theory," *SPE Journal*, vol. 19, no. 6, 2014.

[57] S. Qiao and X. Hu, "Using local IAST with micropore size distribution to predict desorption and displacement kinetics of mixed gases in activated carbon," *Separation and Purification Technology*, vol. 31, no. 1, pp. 19–30, 2003.

[58] F. Dreisbach, R. Staudt, and J. U. Keller, “High pressure adsorption data of methane, nitrogen, carbon dioxide and their binary and ternary mixtures on activated carbon,” *Adsorption*, vol. 5, no. 3, pp. 215–227, 1999.

APPENDIX A

DRA CALCULATIONS RESULTS

This appendix includes tabulated values for all the results of the DRA potential calculations for the adsorption of binary and ternary mixture for CH_4, N_2 and CO_2. The bulk phase conditions were selected based on the experimental data of Dreisbach et al. [58] to eventually compute the deviations between this work and their measurements as illustrated in subsection 5.3.

Table A.1: Results of adsorption calculations for a mixture of CH_4 and CO_2 at $T = 298\ K$ and various pressures and bulk compositions.

Bulk conditions		*Excess quantities*		*Absolute quantities*	
$P\ (MPa)$	x_{B,CH_4}	$\Gamma\ (mol/kg)$	x_{ex,CH_4}	$N_{ads}\ (mol/kg)$	x_{CH_4}
0.102	0.574	1.759	0.319	1.776	0.321
0.100	0.954	1.172	0.913	1.188	0.914
0.500	0.957	3.263	0.900	3.347	0.901
1.025	0.948	4.616	0.868	4.789	0.871
2.149	0.941	6.019	0.839	6.391	0.845
3.097	0.948	6.540	0.854	7.087	0.861
3.887	0.939	6.878	0.826	7.577	0.836
5.108	0.941	7.102	0.828	8.044	0.841
5.916	0.947	7.132	0.845	8.238	0.859

Table A.2: Results of adsorption calculations for a mixture of CH_4 and N_2 at $T = 298$ K and various pressures and bulk compositions.

Bulk conditions		*Excess quantities*		*Absolute quantities*	
P (MPa)	x_{B,CH_4}	Γ (mol/kg)	x_{ex,CH_4}	N_{ads} (mol/kg)	x_{CH_4}
0.151	0.089	0.600	0.290	0.625	0.282
0.522	0.059	1.488	0.205	1.575	0.197
0.974	0.095	2.359	0.298	2.520	0.285
1.925	0.095	3.396	0.295	3.717	0.278
2.969	0.095	4.092	0.293	4.587	0.271
3.930	0.088	4.493	0.274	5.150	0.250
5.056	0.091	4.853	0.281	5.698	0.253
6.035	0.090	5.063	0.278	6.072	0.247
0.111	0.377	0.735	0.724	0.753	0.716
0.533	0.384	2.255	0.725	2.343	0.712
1.039	0.439	3.387	0.767	3.561	0.751
2.285	0.428	4.692	0.758	5.077	0.733
2.764	0.427	4.997	0.757	5.464	0.729
3.977	0.403	5.470	0.740	6.147	0.703
5.980	0.425	5.966	0.762	6.996	0.712
0.518	0.668	2.708	0.896	2.794	0.889
1.091	0.735	4.057	0.922	4.240	0.914
3.972	0.726	6.118	0.922	6.810	0.902
4.986	0.727	6.355	0.925	7.234	0.901
0.108	0.730	0.999	0.922	1.017	0.919
2.023	0.733	5.134	0.922	5.478	0.910
2.978	0.731	5.744	0.922	6.257	0.907
5.975	0.733	6.497	0.929	7.562	0.901
4.987	0.449	5.846	0.778	6.703	0.736

Table A.3: Results of adsorption calculations for a mixture of CO_2 and N_2 at $T = 298$ K and various pressures and bulk compositions.

Bulk conditions		*Excess quantities*		*Absolute quantities*	
$P\ (MPa)$	x_{B,CO_2}	$\Gamma\ (mol/kg)$	x_{ex,CO_2}	$N_{ads}\ (mol/kg)$	x_{CO_2}
0.1082	0.1889	0.8703	0.7357	0.8882	0.7247
0.5351	0.2022	3.0601	0.8030	3.1489	0.7860
1.0584	0.2160	4.6151	0.8368	4.7919	0.8139
1.8750	0.2161	5.9040	0.8532	6.2197	0.8208
3.0781	0.2171	6.9252	0.8709	7.4491	0.8249
4.1020	0.2111	7.3370	0.8764	8.0403	0.8183
5.0660	0.1800	7.4354	0.8337	8.1486	0.7765
6.0771	0.2030	7.6970	0.8868	8.7503	0.8045

Table A.4: Results of adsorption calculations for a mixture of CH_4, CO_2 and N_2 at $T = 298\ K$, various pressures and CH_4 bulk compositions greater than 0.5.

Bulk conditions			*Excess quantities*			*Absolute quantities*		
$P\ (MPa)$	x_{B,CH_4}	x_{B,CO_2}	Γ	x_{ex,CH_4}	x_{ex,CO_2}	N_{ads}	x_{CH_4}	x_{CO_2}
0.103	0.500	0.157	1.120	0.538	0.383	1.137	0.537	0.379
0.485	0.510	0.182	3.400	0.453	0.488	3.481	0.454	0.481
1.073	0.509	0.201	5.175	0.400	0.553	5.357	0.404	0.541
1.999	0.512	0.211	6.564	0.371	0.590	6.908	0.378	0.572
3.008	0.512	0.218	7.348	0.352	0.616	7.877	0.362	0.590
4.016	0.511	0.223	7.771	0.339	0.634	8.492	0.353	0.599
4.957	0.510	0.227	7.985	0.331	0.647	8.891	0.349	0.604
5.991	0.508	0.230	8.090	0.324	0.657	9.207	0.347	0.606
0.107	0.564	0.289	1.508	0.415	0.562	1.526	0.417	0.558
0.433	0.535	0.341	4.018	0.306	0.679	4.090	0.310	0.673
1.054	0.538	0.347	6.107	0.274	0.715	6.286	0.281	0.704
1.996	0.535	0.359	7.566	0.246	0.746	7.916	0.259	0.729
3.023	0.524	0.373	8.334	0.222	0.772	8.881	0.241	0.748
4.025	0.522	0.377	8.668	0.212	0.784	9.420	0.237	0.752
5.034	0.518	0.382	8.810	0.203	0.795	9.783	0.234	0.754
5.861	0.522	0.377	8.798	0.204	0.796	9.960	0.241	0.747
0.093	0.707	0.113	1.077	0.718	0.242	1.093	0.718	0.240
0.478	0.707	0.113	3.230	0.671	0.291	3.310	0.672	0.287
1.030	0.741	0.096	4.632	0.699	0.267	4.806	0.701	0.261
2.003	0.723	0.126	6.133	0.613	0.361	6.478	0.619	0.349
3.022	0.712	0.132	6.861	0.586	0.389	7.392	0.596	0.370
3.834	0.733	0.131	7.192	0.592	0.388	7.878	0.604	0.366
4.937	0.726	0.130	7.415	0.588	0.392	8.316	0.603	0.364
5.837	0.718	0.134	7.529	0.576	0.407	8.612	0.594	0.372

Table A.5: Results of adsorption calculations for a mixture of CH_4, CO_2 and N_2 at $T = 298\ K$, various pressures and CH_4 bulk compositions less than 0.5.

Bulk conditions			*Excess quantities*			*Absolute quantities*		
$P\ (MPa)$	x_{B,CH_4}	x_{B,CO_2}	Γ	x_{ex,CH_4}	x_{ex,CO_2}	N_{ads}	x_{CH_4}	x_{CO_2}
0.102	0.308	0.211	1.108	0.331	0.558	1.125	0.331	0.553
0.467	0.350	0.241	3.486	0.286	0.644	3.564	0.287	0.635
1.017	0.329	0.283	5.447	0.219	0.730	5.618	0.222	0.716
2.009	0.340	0.304	7.116	0.196	0.768	7.462	0.203	0.746
3.011	0.343	0.281	7.698	0.205	0.760	8.226	0.213	0.729
4.001	0.342	0.286	8.116	0.196	0.775	8.832	0.208	0.735
5.017	0.332	0.296	8.377	0.182	0.797	9.293	0.196	0.748
6.013	0.342	0.307	8.509	0.178	0.809	9.633	0.197	0.751
0.113	0.445	0.051	0.911	0.680	0.148	0.930	0.676	0.146
0.525	0.474	0.070	2.817	0.631	0.233	2.904	0.626	0.228
1.111	0.486	0.073	4.200	0.616	0.259	4.387	0.610	0.251
1.986	0.484	0.078	5.345	0.592	0.291	5.681	0.586	0.278
3.012	0.485	0.082	6.108	0.577	0.314	6.626	0.570	0.296
4.011	0.486	0.084	6.544	0.570	0.327	7.241	0.562	0.304
4.964	0.485	0.085	6.788	0.567	0.334	7.660	0.558	0.306
5.798	0.487	0.087	6.937	0.564	0.343	7.964	0.554	0.310